**M-Pos380**

SPECIFIC INTERACTION OF A PARTIALLY PURIFIED XENOPUS TRANSCRIPTION FACTOR IIIC (TFIIIC) WITH FROG tRNA AND TFIIIA GENES

B.S. Shastry and Z.G. Zhang. (intro. by Liboff, Abraham R) Eye Research Institute of Oakland University, Rochester, MI

The dual 5S RNA gene system of Xenopus is an excellent system to study the mechanisms controlling the developmental regulation of eukaryotic genes. One possible experimental approach to understand the differential regulation of eukaryotic genes is to reconstruct the specific transcriptional events in vitro using defined components. This involves the isolation and characterization of the molecules that mediate specific transcription either through protein: protein or DNA-protein interaction or both. Previous studies using a homologous extract from Xenopus indicated that, in addition to RNA polymerase III, all class III genes require two chromatographically distinct fractions (designated TFIIIB and TFIIIC) whereas 5S RNA genes require an additional component TFIIIA. To gain further insight into the mechanisms controlling the cell type specific expression of Xenopus 5S RNA genes and to determine the diversity and specificity of class III gene factors, we have partially purified one of the transcription factors (TFIIIC) by conventional chromatographic methods. This fraction contains an activity which specifically recognizes the "B" block element of the tRNA and TFIIIA gene as demonstrated by DNAase I and/or the chemical method of footpring. Interestingly, two other regions located downstream from the "B" block sequences of tRNA gene are also protected. As evidenced by the gel retardation assay, this complex formation can be quantitatively inhibited by adding excess cold DNA containing "B" block sequence or by heat denaturation of proteins, but not by non-specific DNA (pBR 322), "A" block sequence or 5S DNA. Footprinting analyses with TFIIIA gene indicate that frog TFIIIC can bind to both strands and that the recognition sequence for TFIIIC is surprisingly flexible in that it can bind DNA even when two base pairs in "B" block sequences are changed. Stable complex formation assays with HeLa extract suggest that TFIIIA gene can stably sequester TFIIIC. This inhibition of transcription can be further reversed by the addition of excess TFIIIC fraction. Similar observations were made with the 5S RNA gene transcription. Protection analyses of the 5S gene by DNAase I with TFIIIA and TFIIIC demonstrate that in the presence of TFIIIA, no additional region is protected by TFIIIC implying that TFIIIC may not associate intimately with DNA even in the presence of TFIIIA.

**M-Pos382**

ANALYSIS OF A MYCOPLASMA DNA REPLICATION ORIGIN. Jack Maniloff and Saibal K. Poddar, Departments of Microbiology and Immunology and of Biophysics, University of Rochester, Medical Center Box 672, Rochester, NY 14642.

Mycoplasmas evolved by degenerate evolution from the eubacteria and have the smallest cellular genomes (700-1700 kb). Mycoplasma virus L2 is a temperate virus containing a small double-stranded DNA genome of 11,965 bp. Our previous studies using the Lai-Nathans pulse-labelling method (J. Virol. 61:1909-12, 1987) identified two DNA replication origins in the L2 genome and mapped one to 3.5-4.0 kb (designated ori1) and the other to 8.0-9.5 kb (designated ori2) on the L2 cleavage map. We have used DNA sequence analysis and S1 nuclease sensitivity studies to further identify and characterize these sites. There is a single strong S1 cleavage site in L2 genome which maps at about 3.7 kb. This coincides with a possible stem-loop structure at bases 3712-3736 and (based on sequence analysis data) may indicate the downstream end of the ori1 site. There is also a weak S1 cleavage site in the L2 genome which maps at about 9.5 kb. This site appears to be within an extremely AT-rich region of the genome that is not related to the ori2 site. Sequence analysis shows the L2 genome contains a single 9-base DnaA box (TTATCCACA) located at base 3774, upstream of the S1 cleavage site. There is also a region of repeated bases about 120 bases upstream of the DnaA box. This 40-base repeat region contains 4 copies of a 6-base repeat. The sequence upstream of the repeat region contains several runs of poly A ($A_n$, where n = 3 or 4) with a 10-11 base periodicity, indicative of a curved DNA structure. These characteristics (S1 nuclease cleavage site, DnaA box, repeated sequences, and curved DNA) are similar to those of other eubacterial cellular and viral DNA replication origins and delineate the mycoplasma virus L2 ori1 site. Hence, all elements of this basic DNA replication origin structure have been retained during the degenerate evolution of the eubacteria to the mycoplasmas. A search for analogous characteristics in the L2 genome region expected to contain ori2 is in progress.

**M-Pos381**

## KINETIC STUDIES OF THE T4 POLYMERASE HOLOENZYME: HOLOENZYME ASSEMBLY TIME AND DNA DISSOCIATION RATE

Mark Young*, Todd Capson, Chris Lively, Stephen J. Benkovic, and Peter H. von Hippel*. *Inst. of Molecular Biology, U. of Oregon, Eugene, OR 97403 and Dept. of Chemistry, The Pennsylvania State University, University Park, PA 16803

The T4 DNA polymerase holoenzyme is the active agent in the *in vivo* replication of bacteriophage T4 DNA, having superior polymerizing properties over the core DNA polymerase. This holoenzyme consists of the T4 DNA polymerase in combination with a three-protein accessory ATPase complex. In an effort to understand the assembly and function of the accessory complex in the DNA polymerase holoenzyme, the first rapid kinetic studies on the holoenzyme have been performed. Kinetics of polymerization of a single base or three bases on the 3' ends of oligonucleotide substrates were examined over times ranging from 5 msec to 5 sec. It was found that on these DNA substrates, assembly of the holoenzyme from its separated components is not rapid relative to the binding of the polymerase alone to DNA, so that if all holoenzyme components are mixed with DNA, polymerase binds and adds nucleotides without the accessory complex. Preincubation of the holoenzyme components with a single nucleoside triphosphate plus DNA followed by the addition of a second nucleotide triphosphate shows that holoenzyme assembly takes place over *ca.* 200 msec. Once the holoenzyme assembles, DNA synthesis occurs in a more processive manner than with polymerase alone. This appears to be due to a 20-fold decrease in the dissociation rate of the holoenzyme from DNA relative to that of core polymerase. Thus an early hypothesis that the accessory complex acts as a "clamp" to hold the polymerase onto DNA is supported. Since it is thought that the role of the accessory complex ATPase is in assembly of the holoenzyme, rapid kinetic studies of the accessory complex ATPase to connect this 200 msec assembly time to steps in the ATP hydrolysis cycle are ongoing.

**M-Pos383**

HYDRATION-DEPENDENT GLASS TRANSITION IN PLANT SEEDS. RELEVANCE TO ANHYDROUS BIOLOGY. F. Bruni, and A.C. Leopold, Dept. of Plant Biology, Cornell University, Ithaca, NY 14853

The means by which anhydrobiotic organisms, such as plant seeds, pollen grains, bacteria, and animal cysts, can survive severe dehydration for long periods of time presents an interesting and difficult problem. Here we report on spin-probe ESR measurements of cytoplasmic viscosity, and on thermally stimulated depolarization experiments undertaken to detect the onset of a vitrified state in plant seeds. We have measured the rotational diffusion coefficient of a hydrophilic spin probe, inserted in the cytoplasm of soybean axes, as a function of temperature. Additionally, the relaxation mechanisms of specific populations of water molecules have been investigated over a range of temperatures and sample water contents. Results obtained with both techniques indicate the existence of a hydration dependent glass-like transition occurring at physiological temperatures. No glass transitions have been observed in desiccation intolerant samples, suggesting that the ability to withstand dehydration is associated with cytoplasmic glass formation.

**M-Pos384**

CYCLIC DEEP FREEZING AND THAWING INDUCES SUGAR CRYSTALLIZATION IN EXTREMELY COLD HARDY POPULUS HIRSH, A.[1], BENT, T.[2] and ERBE, E.[3]. American Red Cross, Rockville, MD[1], Comsat Corp., Clarksburg, MD[2], USDA ARC, Beltsville, MD[3]

*Populus balsamifera v. virginiana* (Sargent) resists a single cycle of cooling to -70°C at rates <5°C per hour in midwinter. If the tissue is continuously cooled and warmed 6x between 0°C and -20°C at these rates it remains uninjured. If it is cooled and warmed 6x at the same rates between -20°C nd -70°C it also remains uninjured. However, *Populus* cooled and warmed at <5°C/hr 6x between 0°C and -70°C is completely killed. Analysis of the latter group of twigs by electron microscopy (EM) shows that (1) plasma membrane looks normal, (2) internal membranes are blebbed and MAPs abnormally distributed, (3) the cytoplasm is filled with small aparticulate vesicles, some intercalated, and (4) no ice forms in the cells. Analysis by dynamic mechanical analysis (DMA) shows that the sugar glass transition peak disappears indicating crystallization of intracellular sugars out of solution. These results lend support to the idea that low molecular weight sugars protect cellular membranes from dehydration stresses *in vivo*, but they indicate that internal membranes are mores susceptible to damage than plasma membrane in *Populus*. Tissue remains uninjured unless the entire range from 0°C to -70°C is repeatedly traversed. We believe this indicates that sugar crystallization is seeded at a limited number of sites at very low temperature and subsequently proceeds to only a limited extent during warming through high subzero temperature during any given cycle. The crystallization may occur because a dilute sugar phase forms in close association with proteins as a result of intracellular phase separation of proteins and sugars during freezing. *This work is supported by NIH grant GM17959.*

**M-Pos385**

HEAT SHOCK, LETHALITY AND MUTAGENESIS IN SACCHAROMYCES CERVISIAE. D. Keszenman, E.C. Candreva, V.A. Salvo, E. Barrios, U.Gelos and E. Nunes. (Intro. by J.A. Connor) Dept. of Biophysics, School of Medicine, Montevideo, Uruguay.

Heath shock proteins (HSP) are translated or activated by hyperthermia (HT) and other environmental perturbations eliciting thermotolerance. This response has been detected in all biological systems so far analyzed and it is considered a model for genetic regulation.

We have analyzed lethal and mutagenic effects of hyperthermia (50° C during different exposure times (t) in stationary cell populations. Part of the samples were exposed to a previous heath shock (38° C, 1-2 h) in culture medium with and without cycloheximide (CHM, 10 ug/ml). An haploid yeast strain auxotropic for lysine was employed (SC7k lys) as well as conventional culture and ommision media (incubation temperature 30° C)

Main results and interpretations are: 1) Low thermotolerance was detected for heath shock lasting 2 h, independently of the presence of CHM. In order to analyze this fact it should be considered that thermoresistance is constitutively expressed after the diauxic switch in these cells. However, the HSP are mainly induced during logarithmic phase after heath shock. 2) The mutagenic frequency M(t) shows an exponential course for t = 30 min and decreases for samples pretreated with heat shock while CHM reverts this effect. These facts suggest that HSP protects DNA from the mutagenic effect of HT and that CHM, as an inhibitor of protein synthesis, counteracts at least in part the effect of heat shock in our experimental conditions.

M-Pos386

COMPARATIVE PHOTOSENSITIZING PROPERTIES OF TIN AND ZINC PORPHYRIN INHIBITORS OF HEME OXYGENASE.
Nancy L. Greenbaum and Attallah Kappas, The Rockefeller University, New York, N.Y. 10021.

A number of synthetic metalloporphyrin analogs of heme are competitive inhbitors of heme oxygenase and thus of bilirubin formation, and are being considered for use in the treatment of neonatal jaundice. These compounds also possess the ability to photosensitize tissue damage in vivo. To assess their photosensitizing properties, the relative production of $^1O_2$ mediated by Sn-proto- (SnPP), Sn-meso- (SnMP), Sn-diiododeutero- ($SnI_2DP$), and Zn-mesoporphyrin (ZnMP) was measured by the rate of $O_2$ uptake associated with reaction with oxidizable substrates. Porphyrin solutions were illuminated by continuous light in the Soret or visible regions of absorption. In aqueous buffer, the Sn compounds (a mixture of monomer and more aggregated forms) sensitized a rapid rate of substrate oxidation; illumination of ZnMP, which was highly aggregated, resulted in no measurable $O_2$ uptake. After dispersion in Triton micelles, the predominantly monomerized ZnMP mediated a rate of $O_2$ uptake approximately 25% faster than did SnMP or SnPP. To simulate the environment in serum, porphyrins were incubated with human serum albumin (HSA), which resulted in spectral shifts indicative of increased monomer formation. Illumination of SnPP or SnMP bound to HSA in buffered solution resulted in a high rate of $O_2$ uptake, but the rate mediated by $SnI_2DP$ was substantially less (3-9 times, depending upon the buffer). The initial rate of $O_2$ uptake sensitized by ZnMP bound to HSA was slightly greater than for the Sn analog. There was no significant destruction of the Sn compounds bound to HSA during the illumination period; however, ZnMP was extremely photolabile, and the resultant oxidation product was ineffective as an inhibitor of heme oxygenase.

M-Pos387

HEMATOPORPHYRIN DERIVATIVE BINDING AND PHOTOINACTIVATION OF HUMAN CEREBRAL GLIOMA CELLS IN CULTURE.

K.Joshi, P.Joshi, and N.B. Joshi, Department of Biophysics, NIMHANS, Bangalore-560 029, (INDIA)

Hematoporphyrin derivative (Hpd) in combination with light is being used in the detection and treatment of malignant diseases. Though the initial results of clinical trials are encouraging the exact mechanism of localization and site of damage is not yet clear. Hematoporphyrin derivative (Hpd) binding and its photodynamic action on human cerebral glioma cells in culture were investigated. The cells were cultured at 37°C in DMEM containing 5% serum and antibiotics. Hpd binding was studied by quantitating the amount of Hpd extracted from the cells and by measuring the fluorescence spectra of cell bound Hpd. The photodamage was assessed by measuring cell survival. The photodamage is highly dependent on the time of incubation. Fluorescence spectrum of cell bound Hpd exhibited three emission bands at 616, 636 and 678 nm. An increase in fluorescence intensity of 636 nm band was observed on increasing incubation time. The Hpd uptake and photosensitivity depends on the growth phase of cells. Plateau phase cells showed an enhanced emission at 636 nm as well as enhanced photosensitivity as compared to exponentially growing cells. Our results suggest that the higher photodamage of exponential phase cells on increasing incubation time as well as in plateau phase cells is due to increased accumulation of Hpd component emitting at 636 nm. This fluorescence band is due to increased accumulation of oligomeric active component of Hpd bound to the hydrophobic sites in the cell.

M-Pos388

A MODEL OF RADIATION ACTION
J.Y. Ostashevsky, SUNY-Health Sci. Ctr. Bklyn, Brooklyn, NY 11203

A model of radiation action was proposed which related the surviving fraction of irradiated cells to unrepaired DNA double-strand breaks (DSB) and DNA fragments. Effects of delayed-plating, inhibitors of DSB repair, hypertonic salt solution, dose fractionation, dose-rate and high-LET radiation were considered in the framework of this model for two possible types of DSB repair: cooperative vs noncooperative. The slowest rate-limiting step in DSB repair is related to a DSB for noncooperative, and to a DNA molecule for cooperative, repair. It is shown that the calculated values (DSB repair time constant, the average dose for induction of one DSB per DNA molecule, the time available for DSB repair, dose and time-dependencies of cell surviving fraction under various postirradiation conditions, dose-dependence of chromosome aberrations and PCC fragments) agree with the experimental data when cooperative rather than noncooperative DSB repair was assumed in the model.

The work was supported by grants R01CA39045 and R01GM43374 from NIH, DHHS.

M-Pos389

TIME RESOLVED ABSORPTION STUDIES AND GLOBAL ANALYSIS ON NATIVE OAT PHYTOCHROME

Chian-Fan Zhang, Sofie Bjorling and David Kliger, Department of Chemistry and Biochemistry, University of California, Santa Cruz, CA 95064
David Farrens and Pill-Soon Song, Department of Chemistry, University of Nebraska, Lincoln, NE 68588

The phototransformation kinetics of native oat phytochrome from *Avena sativa* are investigated by laser photolysis experiments at 10 °C. The photoreaction from the red absorbing form (Pr) to the far red absorbing form (Pfr) is initiated by 7 ns (fwhm), 650 nm laser pulses. Transient absorption difference spectra in the UV and visible regions are recorded by a gated optical multichannel analyzer system from nanoseconds to seconds after photolysis. The data are analyzed by using singular-value decomposition (SVD) and global exponential fitting to determine the number of intermediates and the decay time constants of the photoreactions. The global fitting of transient spectra data is used to evaluate various kinetic models of the interconversion of Pr, Lumi-R, Meta-Ra, Meta-Rc, and Pfr.

**M-Pos390**

## SITE-DIRECTED MUTAGENESIS OF THE ELECTRON-TRANSFER SUBUNIT OF *Escherichia coli* DIMETHYLSULPHOXIDE REDUCTASE

Richard A. Rothery and Joel H. Weiner. (Intro. by Joyce R. Pearlstone.) Department of Biochemistry, University of Alberta, Edmonton, Canada.

*Escherichia coli*, when grown anaerobically with DMSO as respiratory oxidant, develops a respiratory chain terminated by DMSO reductase. This enzyme consists of three subunits: a molybdopterin-containing catalytic subunit (DmsA), an [Fe-S] electron-transfer subunit (DmsB), and a membrane-anchor subunit (DmsC). DmsB contains 16 Cys residues arranged in four groups (I-IV), three (I-III) of which have sequences typical of the Cys groups ligating the [4Fe-4S] clusters of many bacterial ferredoxins [Bilous, P. *et al.* (1988). *Molec.Microbiol.*, **2**, 785-795]. Group IV has no homology with known ferredoxin sequences, although there is EPR evidence that Cys groups I-IV ligate four [4Fe-4S] clusters [Cammack, R. & Weiner, J.H. (1990). *Biochemistry*, **29**, 8410-8416]. Significant sequence homologies exist between DmsB and *E.coli* nitrate reductase subunit β [Blasco, F. *et al.* (1989). *Mol.Gen.Genet.*, **218**, 249-256]. The latter enzyme also contains four groups of Cys residues, but the group corresponding to group III of DmsB has a sequence similar to the Cys groups ligating [3Fe-4S] clusters in many bacterial ferredoxins. This group has a Trp ($W_{220}$) substituted for the second Cys ($C_{102}$) present in DmsB group III. We have used site-directed mutagenesis to effect the change $C_{102} \rightarrow W_{102}$ in the sequence of DmsB and show by EPR that this results in the assembly of a [3Fe-4S] cluster into the mutant enzyme in place of the [4Fe-4S] cluster ligated by Cys group III in the wild-type enzyme. We have also effected the change $C_{102} \rightarrow S_{102}$ and show that this also results in the formation of a new [3Fe-4S] cluster. Mutant enzymes with Ser or Trp in place of $C_{102}$ do not support respiratory growth with DMSO as terminal oxidant. Mutations in other Cys residues in DmsB do not result in the formation of new [3Fe-4S] clusters.

Supported by the Medical Research Council of Canada and the Alberta Heritage Foundation for Medical Research.

**M-Pos391**

## THE USE OF ELECTRON PARAMAGNETIC RESONANCE SPECTROMETRY IN THE IDENTIFICATION OF THE FREE RADICAL SPECIES RESPONSIBLE FOR ARYLAMINE-INDUCED HEMOLYTIC ANEMIA

T.P. Bradshaw, D.C. McMillan, R.K. Crouch and D.J. Jollow. Medical University of South Carolina; Charleston, South Carolina.

Electron paramagnetic resonance (EPR) spectrometry and the spin trapping agent, 5,5-dimethyl-1-pyrroline-N-oxide (DMPO), were utilized to examine the role of free radical species in the events leading to arylamine-induced hemolytic anemia. Phenylhydroxylamine (PHA), a direct-acting hemolytic agent, in the presence of DMPO and lysed or intact rat erythrocytes gave rise to a four line (1:2:2:1) EPR spectrum consistent with the trapping of either a hydroxyl free radical (·OH) or glutathione thiyl (·SG) radical. No signal was obtained in control experiments in which either PHA, DMPO, or red cells were omitted. The hyperfine coupling constants measured from the photolytic generation of both the DMPO-OH and DMPO-SG adducts allowed the PHA-induced species to be identified as the ·SG free radical. Confirming evidence was provided by the rapid removal of glutathione (GSH) from a red cell hemolysate by pressure-filtration. After the filtration step, the control DMPO-SG signal was abolished; however, addition of exogenous GSH resulted in its return.

To examine a possible role for active oxygen species in the generation of the ·SG radical, the following studies were conducted: 1) the addition of DMPO to a xanthine/xanthine oxidase model system resulted in the appearance of the DMPO-OH EPR signal when carried out with or without lysed red cells; no signal occurred when the xanthine oxidase was excluded; 2) superoxide dismutase (SOD) (1890 units) and catalase (1680-2600 units) suppressed the DMPO-OH signal generated by the xanthine/xanthine oxidase model system, both in the presence and absence of the red cell lysate with similar suppression observed in the PHA-generated ·SG signal, albeit at higher enzyme levels; 3) the removal of oxygen from the red cell hemolysate-DMPO reaction mixture prior to PHA addition prevented the development of the four-line EPR signal.

Collectively, these studies indicate that both active oxygen and thiyl free radical species are involved in the spin-trapping with DMPO. The data are consistent with the postulate that active oxygen species generated by the interaction of PHA with oxyhemoglobin leads to the formation of thiyl radical species which, via disulfide bridge formation, leads in turn to modification of red cell protein structure/function. (This work was supported by NIH grants HL30038 and EY05757)

**M-Pos392**

## THE $^{15}N$- AND $^{2}H$-SUBSTITUTED MALEIMIDO TEMPO SPIN LABEL DETECTS CROSS-BRIDGE ROTATION AS A CHANGE IN THE TORSION ANGLE OF THE SPIN PROBE.

K. Ajtai and T. P. Burghardt, Department of Biochemistry and Molecular Biology, Mayo Foundation, Rochester, MN 55905, U.S.A.

From studies of muscle fibers decorated with MTSL-S1, we concluded that the cross-bridge rotates upon binding MgADP in a manner that rotates the spin probe about its torsion angle. This conclusion is not evident from the EPR spectra measured from the decorated muscle fibers, but was deduced from a detailed model-independent study of the spectral shape. In order to increase the EPR signal and enhance the angular resolving power of the spin label, $^{15}N$ and $^{2}H$ substituted maleimido TEMPO was used in the present studies (gift from Dr. A. Beth, Vanderbilt University, Nashville, TN). The replacement of $^{15}N$,$^{2}H$ near the nitroxide group in spin labels decreases the spectral linewidth by reducing proton broadening and consequently increases the signal-to-noise for the detection of the EPR signal by ~5 fold. The narrowed linewidth also enhances the resolution of the spin probe angular distribution determined from the EPR spectrum. Replacing $^{14}N$ with stable isotope $^{15}N$ in the nitroxide group increases the signal-to-noise by an additional factor of ~2 and further enhances the angular resolution by reducing the spectral overlap that leads to orientation ambiguities. We investigated the rotation of actin bound myosin cross-bridges, that occurs when the cross-bridges also bind MgADP, using [$^{15}N$,$^{2}H$]MTSL-S1 decorating muscle fibers. We wanted to see if the substituted probe could more readily detect this rotation. Our data confirms our earlier conclusion and demonstrates that EPR spectra from [$^{15}N$,$^{2}H$]MTSL-S1 decorated fibers perpendicular to the Zeeman field show an evident change, due to the nucleotide binding to the cross-bridge, that can be directly attributed to a large change in the torsion angle of the probe. Supported by grants from NSF (DMB 8819755) and NIH (1 401 AR 39288-01A2). T.P.B. is an Established Investigator of the American Heart Association.

**M-Pos393**

## THE ANGULAR TRAJECTORY OF THE FLUORESCENCE TRANSITION DIPOLES OF 1,5-IAEDANS LABELING MUSCLE FIBERS AS A FUNCTION OF EXCITATION AND EMISSION WAVELENGTHS.

A. Ringler, K. Ajtai, and T. P. Burghardt, Department of Biochemistry and Molecular Biology, Mayo Foundation, Rochester, MN, 55905, U.S.A.

The fluorescence polarization spectrum from 1,5-IAEDANS and the electron paramagnetic resonance spectra from $^{15}N$ and $^{2}H$ substituted (maleimido)TEMPO spin label ([$^{15}N$, $^{2}H$]MTSL) and (iodoacetamido)PROXYL spin label (IPSL), modifying myosin sulfhydryl 1 in muscle fibers, were interpreted in terms of probe order parameters using a model-independent method. The order parameters are related to each other by an Euler rotation of coordinates. This relationship links the sets of order parameters from the different probes and gives rise to a system of equations that are solved to give the Euler angles relating the different probe coordinate frames. From these Euler angles we find that we can plot the angular trajectory of the transition dipoles of 1,5-IAEDANS as a function of the excitation and emission wavelengths. The angular trajectories are helpful in interpreting data from probe modified biological assemblies. The implications for myosin cross-bridges in muscle fibers will be discussed. Supported by NSF (DMB 88-19755), NIH (R01 AR 39288), and the AHA (900644). T.P.B. is an Established Investigator of the American Heart Association.

**M-Pos394**

$^{13}C$ NMR STUDIES OF GLYCINE BETAINE AND TREHALOSE AS PROBES OF THE CYTOPLASM OF *ESCHERICHIA COLI* K12 Harry J. Guttman, Barbara A. Lewis, D. Scott Cayley, Vera M. Kolb+, Veronica Brushaber, Charles F. Anderson, and M. Thomas Record, Jr. Departments of Chemistry and Biochemistry, University of Wisconsin - Madison, Madison WI 53706, +Department of Chemistry, University of Wisconsin - Parkside, Kenosha WI 53141

It has been our laboratory's recent objective to quantitatively characterize the intracellular environment of *Escherichia coli* K12. Our measurements establish the feasibility of determining the abundance and motional properties of osmolytes within the cell.

When *E. coli* K12 are grown in high osmolarity media containing betaine (glycine betaine), the cells transport betaine from the medium into the cell. The accumulation of betaine stimulates growth in osmotically stressed cells. Hence, betaine is termed an "osmoprotectant". In high osmolarity media without betaine, the cells synthesize the disaccharide trehalose.

We have measured the relaxation rates and the Nuclear Overhauser Enhancements of betaine and trehalose *in vivo* and in various *in vitro* model systems. From the small differences between *in vivo* and *in vitro* correlation times, we infer that there is no binding of these osmolytes to macromolecules in the cell. This is consistent with the thermodynamic role osmolytes play in the cell (i.e. remaining osmotically active *in vivo*). Extension of the present study to other *in vivo* and *in vitro* conditions will ultimately permit a more detailed physical description of the intracellular environment of *E. coli* and of its changes in adapting to extreme growth conditions.

Supported by NSF CHE88-03673.

**M-Pos395**

Deuterium and Phosphorus NMR Studies of Sphingomyelin Microemulsions Containing Cholesteryl Oleate or Triolein.

W. Dale Treleaven, Robert J. Cushley, and Lisa Zhao Department of Chemistry, Simon Fraser University, Burnaby, British Columbia, Canada V5A 1S6.

Microemulsions containing a sphingomyelin monolayer, and a neutral lipid core of either cholesteryl oleate, or triolein were prepared by sonication at pH 8.4, against a background density of 1.25 g/ml. Following sonication, density of the solution was reduced to 1.005 g/ml by dialysis, and unilamellar vesicles were removed by ultracentrifugation. Phosphorus NMR experiments, in the presence of manganese chloride, were conducted in order to monitor the residual contamination of non-microemulsion structures. Mean particle size, determined by quasi-elastic light scattering, was 25-27 nm. Molecular order within the neutral lipid core was monitored by deuterium NMR over the range 5-55 $^{0}C$ The effect of core composition on the dynamic structure of the microemulsion surface was monitored by phosphorus NMR.

**M-Pos396**

**EXAMINATION OF THE STRUCTURE OF LECTIN-BOUND OLIGOSACCHARIDES USING TRANSFERRED NOES**

Vicky L. Bevilacqua and James H. Prestegard

Cell surface oligosaccharides often serve as receptors for proteins involved in membrane surface recognition or transmembrane communication. The conformations of these oligosaccharides when complexed with a protein are, therefore, of considerable importance in understanding receptor function. We present some NMR-based methods for the study of simple oligosaccharides in this protein-bound form and illustrate them with galactose-terminated ligands bound to the ricin B-Chain, a plant lectin. The methods used include selective deuteration and spin simulation to aid in the interpretation of transferred nuclear Overhauser effect NMR experiments on mono- and disaccharides when bound to the ricin B-Chain (Rb). A conformational change has been seen for β-methyl lactoside upon binding to Rb which indicates the selection of one conformer from a range of conformers existing in solution. Insight into the importance of the type of glycosidic linkage will be provided by a comparison of the results for β-methyl lactoside, which contains galactose linked β-1-4 to glucose, with the results for melibiose, which contains an α-1-6 linkage between galactose and glucose.

**M-Pos397**

MULTINUCLEAR SPIN RELAXATION STUDIES OF SOY GLOBULIN HYDRATION, ION-BINDING AND PROTEIN ACTIVITY IN RELATION TO RHEOLOGICAL PROPERTIES IN SOLUTION. T.C. Wei*+, S.Yenerich* and I.C. Baianu*+, *University of Illinois at Urbana, Dept. of Food Science, +AFC-NMR Facility, 580 Bevier Hall, 905 S. Goodwin Avenue, Urbana, Illinois 61801.

Measurements of nuclear spin relaxation rates of water or $D_2O$ in soy globulin solutions were carried out as a function of protein concentration, pH and salt concentration. A comparison of $^{17}O$ and $^{2}H$ NMR relaxation rates of water and $D_2O$ allowed the separation of the chemical exchange contribution of deuterons to the $^{2}H$ NMR relaxation from the hydration and activity effects. Scaled, $^{1}H$ and $^{2}H$ NMR relaxation rates allowed the determination of the cross-relaxation contribution to the $^{1}H$ NMR relxation in such systems, as a function of protein concentration and pH. Protein and salt activities were determined by non-linear regression analysis of the data with an Apple-Macintosh II microcomputer. Ion-binding was studied for the following salts,added to the soy globulin solutions: NaCl, LiCl, CsCl, NaBr, NaI and $Na_2SO_4$, at both pH 7.3 and 11.0. Both the NMR relaxation and the rheological results at pH 7.3 are in very good agreement with an ion-binding/isoelectric precipitation model [1]. The separate contributions of cations and anions to salting-in and salting-out of soy globulins were determined for the first time with this model. The observed behavior of soy globulins at high pH was dominated by the titration of the arginine and lysine groups. The hydration of soy globulins increased from 0.33g $H_2O$ / g soy globulins at pH 8 to 0.52 at pH 11. At pH 11.5, the second virial coefficient, $B_o$, of soy globulins was 5.8 ml/g. The average correlation time of water molecules hydrating soy globulins was calculated to be 16 ps from $^{17}O$ NMR relaxation data at pH 11 and 22°C, by assuming a fast-exchange model for water with only one type of motions. This value is consistent with the correlation times of Arg $C_\zeta$ and Lys , determined previously by $^{13}C$ NMR studies of soy glycinins in $D_2O$.

REFERENCES CITED:

1. T.F. Kumosinski, J. Agr. Food Chem., 36 :669 (1988).
2. L.T. Kakalis and I.C. Baianu, J. Agric. Food Chem., 37: 1222-1228 (1989).

**M-Pos398**

$^{13}C$ MAGIC-ANGLE SPINING NMR AS A SOURCE OF DYNAMIC INFORMATION FOR MEMBRANE SYSTEMS. Paul J.R. Spooner, Leon Van Gorkom† and Anthony Watts. Department of Biochemistry, University of Oxford, South Parks Road, Oxford OX1 3QU, U.K. and †Department of Biochemistry, McMasters University, Health Sciences Center, Hamilton, Ontario, Canada.

$^{13}C$ MAS NMR has been investigated as a means of obtaining information on the molecular dynamics within phospholipid bilayer membranes and protein-lipid complexes. Preliminary studies on hydrated bilayers of dipalmitoyl phosphatidylcholine show that MAS generates well resolved natural abundance $^{13}C$ NMR spectra even for lipid in the gel state. The rotational side-band intensities observed at slow rotation (1.1 kHz) clearly define the bounderies of the gel→liquid-crystalline thermotropic phase transition of the lipid and show that the high-power irradiation used in these experiments for cross-polarization (CP) or proton-decoupling can be adjusted to produce only moderate heating effects in typical membrane samples. The technique has been extended to the analysis of protein-lipid systems for which CP with lengthy contact times (1-30 ms) was used to derive highly resolved $^{13}C$ spectra from the lipid components. Variable contact-time CP MAS experiments provide profiles of the CP build-up and decay which reflects the strength of $^{1}H$-$^{13}C$ dipolar interactions as well as the magnitude of $^{13}C$ relaxation in the rotating-frame which are both a function of the degree of motional averaging for lipid in these bilayer systems. Results indicate that cytochrome *c* binding to cardiolipin bilayers generally restricts motional re-orientation in the lipid except for the poly-unsaturated region of the fatty acyl chains, where motion appears to be selectively enhanced. The incorporation of the M13 coat protein into lipid bilayers also restricted overall lipid motion, but appeared to produce an increase in the motional freedom for the headgroup methyl groups of DMPC, in agreement with other spectroscopic results. These results demonstrate the advantage of this approach in identifying dynamic events apparently localized to specific regions of membrane molecules.

**M-Pos399**

SPIN TRAPPING OF FREE RADICALS PRODUCED DURING RAT LIVER ISCHEMIA-REPERFUSION INJURY.
Yoshiki Takehara*, S. Tsuyoshi Ohnishi**, Tomoko Ohnishi* and Tamotsu Yoshioka*** (Intro. by T.M. Devlin)
*Dept. of Biochem. Biophys. Univ. of Penna. Phila. PA 19104, **Philadelphia Biomedical Res. Inst., Radnor, PA 19087 and ***Center for Adult Diseases, Kurashiki, 710 Japan.

It has been theorized that ischemia-reperfusion of the liver produces oxygen free radicals, and that these radicals impair cellular components such as lipids and proteins. However, the direct proof of free radical production has not been provided. We have succeeded in detecting oxygen free radicals in a rat liver ischemia-reperfusion model. After ischemia/reperfusion, the liver was homogenized in a buffer solution containing PBN, a spin trapping agent. From the Folch extract, we were able to detect the spin adduct of free radicals. The lipid peroxidation was evaluated by measuring TBA reactive substances during ischemia and reperfusion.

We found that both free radical formation and lipid peroxidation were not induced by ischemia alone. However, upon reperfusion, EPR signals of spin adduct abruptly appeard and reached a peak in 1-2 minutes. Lipid peroxidation slowly increased and reached a peak around 10-20 minutes. The peak intensities of both free radicals and lipid peroxidation increased with the increase of ischemia time. There was a correlation between the free radical formation and the lipid peroxidation, suggesting that the production of free radicals may be a trigger of lipid peroxidation. The effects of free radical scavengers are being studied.

**M-Pos400**

**MSL Spin Labelling ESR Spectrum Study of the Toxic Effects of Cadmium on Protein Thiol Microenvironment and Protein Fluidity of Human Erythrocyte Membrane in Vitro.** Yunbo Li*, and Shijie Liu, * Dept. of Molecular and Cell Biology, University of California, Berkeley, CA 94720; Dept. of Occupational Health, Beijing Medical University, Beijing 100083, P.R. China.

On the basis of our previous studies, 3-Maleimide-PROXYL(MSL) spin labelling ESR spectrum was used in this study to deeply clarify the toxic effect of cadmium on protein thiol microenvironment and protein fluidity of human erythrocyte membrane. Erythrocytes were treated with cadmium(40 and 160 μM) for 2 hours and then labelled with MSL, showing decreases of W and S values and the S/W ratio, with dose-effect and time-effect relationships. These indicate that cadmium could change the microenvironment of protein thiol of erythrocyte membrane, resulting in the decrease of MSL combined with thiol groups. Spin related time of membrane proteins calculated by ESR spectra was shorter in cadmium treated erythrocytes than in control, which revealed that cadmium could increase the membrne protein fluidity of erythrocytes. Simultaneously with cadmium exposure adding DTT could partly prevent the changes of W, S, S/W ratio and spin related time of membrane proteins, which further indicates the effects of cadmium on membrane protein thiol groups of erythrocytes.

**M-Pos401**

BINDING OF ATP TO UNCOUPLING PROTEIN (UP) OF BROWN FAT MITOCHONDRIA AS STUDIED BY MEANS OF SPIN-LABELED ATP DERIVATIVES.
P. Jakobs, P. Jezek and W.E. Trommer, Department of Chemistry, University of Kaiserslautern, FRG, and Institute of Physiology, Czechoslovak Academy of Science, Prague, CSFR.

Mitochondrial respiration and oxidative phosphorylation are uncoupled by UP-mediated $H^+$ transport across the inner mitochondrial membrane. Besides protons, chloride ions are translocated, as well. Adenine nucleotides are inhibitors of these processes. ATP, spin-labeled (SL) at C8 of the adenine ring was found to inhibit $Cl^-$ transport almost as strongly as ATP itself ($K_i$=9.6 μM as compared to 4.6 μM).

C8-SL-ATP binds tightly to UP as revealed by ESR spectra typical of immobilized species and a concomitant decrease in the signal amplitude of the freely tumbling SL-nucleotide. Detailed binding studies at pH 6.3 yielded a $K_d$ of 45 μM with a stoichiometry of one per dimer. At pH 7.5 this value was about 10-fold higher. Addition of 2 mM $Mg^{2+}$ reduced binding considerably (3-fold). An unmodified ribose moiety of ATP appears to be required for tight binding as an ATP derivative spin-labeled at the ribose was hardly bound at all.

UP derivatized with N-ethylmaleimide (NEM) or diazobenzenesulfonate has been known to loose the inhibition by ATP. However, the NEM-modified enzyme still bound one equivalent of C8-SL-ATP per dimer, although 7-fold weaker ($K_d$=300 μM).

**M-Pos402**

A RE-INVESTIGATION OF CHROMATIUM VINOSUM HIGH-POTENTIAL IRON-SULFUR PROTEIN BY EPR AND MOSSBAUER SPECTROSCOPY. W.R. Dunham, W.R. Hagen, J.A. Fee, and R.H. Sands, Biophysics Research Division, The University of Michigan, Ann Arbor, MI 48109-2099.

The High-Potential Iron-sulfur Protein (HiPIP from Chromatium vinosum is the classical example from a class of small redox proteins in which the cubane prosthetic group shuttles between the one-electron and the two-electron reduced forms, i.e. [4Fe4S]3+;2+. We have re-investigated this protein with EPR and Mossbauer spectroscopy in order to re-establish some of its properties by present-day standards. The long-standing triple-species model [B.C. Antanaitis and T.H. Moss (1975) Biochim. Biophys. Acta, 305, 262-279], which interprets the EPR as a sum of three components and which relates the two major ones of these to observables in NMR and Mossbauer spectra, is argued to be incorrect. Instead, we find that the EPR is more satisfactorily explained as a sum of two components, a major one with g=2.02; 2.04; 2.12, and a minor one with g=2.04; 2.07; 2.13. The two components presumably represent independent spin systems both with a ground state of S=1/2. The spectral shapes (including g-tensors) and relative intensities of the two S=1/2 systems are functions of the solvent composition, e.g., can be influenced by the addition of organic solvents or salt. In the presence of 0.1-2.0 M NaCl, freezing induces polymerization (probably dimers) of the protein, which is detected as inter-cluster spin-spin interaction in the EPR. The interaction can be prevented by rapid freezing or by partial oxidation. The latter method statistically favors the occurrence of dimers in which only one cluster of a potentially interacting pair is paramagnetic. The computer simulation of the spectra at X-band and Q-band show that the inter-site vector and the magnetic z-axis are along the line from the cubane to the nearest approach of the protein surface and that this line is also along the 3-fold axis of the cubane.

M-Pos403

OPTICAL MAPPING OF MOTION ON AN ATOMIC SCALE*
Hungyi Lin and Mark Sharnoff, Department of Physics, University of Delaware, Newark, DE 19716

Our holographic methods for the study of ultramicroscopic motion of particulate matter are now able reliably to register and to image displacements as small as 3 ångstrom units. In our most recent experiments the "particles" are small bubbles of air drifting at speeds of ≈0.3 mm/hour in a nearly horizontal capillary filled with glycerine. A millimetric scale placed beside the capillary serves to calibrate their displacements, and periodic observations made over several hours show the bubble trajectories to be smooth and rectilinear. A bubble known to be stationary is included as a fiducial point in each scene. A laser beam illuminates the bubbles obliquely, and the scattered light is collected by a low power microscope before transmission to the holographic plate. Two reference waves, each doubly flashed, also illuminate the plate, and these serve to record a pair of double-exposure holograms simultaneously. The holograms of each pair are phase-unbalanced conjugates (Lin and Sharnoff, Appl. Optics, Nov., 1990). After collation, the conjugate phase-unbalanced images reconstructed from them are acquired sequentially by a CCD camera and processed electronically. Common-mode details are removed by digital subtraction, which normally renders the stationary fiducial bubble invisible. The brightness with which the moving bubbles appear is proportional to their respective drift speeds, and the brightness of any bubble increases monotonically and approximately linearly with interflash interval as the latter is varied over the range from 4 to 16 msec.

* Supported by NSF under DCB 8821065.

M-Pos404

OPTICAL SPATIAL INTENSITY PROFILES IN TOTAL INTERNAL REFLECTION.
James R. Abney*, Bethe A. Scalettar*, and Nancy L. Thompson†. *Department of Cell Biology & Anatomy and †Department of Chemistry, University of North Carolina, Chapel Hill, NC 27599.

When light propagating through a medium of higher refractive index is incident on a medium of lower refractive index, the phenomenon of total internal reflection (TIR) can occur for incidence angles greater than the "critical angle" [Axelrod et al., *Ann. Rev. Biophys. Bioeng.* 13:247 (1984)]. Under such conditions, all of the light is reflected, but an electromagnetic field known as the "evanescent wave" penetrates a short distance into the second medium. This field can be used to excite fluorescence near the interface and is the basis of techniques such as TIR fluorescence microscopy (TIRFM), TIR/fluorescence photobleaching recovery (TIR/FPR), and TIR/fluorescence correlation spectroscopy (TIR/FCS). In this study the optical spatial intensity profile (or "interference pattern") of the evanescent field generated by two colliding monochromatic waves is derived. The pattern depends on the refractive indices of the two media, the intensities and polarizations of the two waves, and the angles of incidence of the two waves relative to the interface and each other. The pattern differs considerably from that obtained when two plane waves interfere *in vacuo* because the evanescent wave, in general, is not transverse. The contrast and periodicity of the interference pattern under various conditions are calculated. These calculations reveal that properly designed colliding beam experiments should permit one to confirm the polarization properties of evanescent fields. Applications of evanescent interference patterns to TIR/FPR are also discussed.

This work was supported by NIH grant GM-37145.

M-Pos405

AN OPTICAL AND ELECTRONIC HETERODYNING TECHNIQUE FOR USE WITH CCD CAMERAS AND ARRAY DETECTORS FOR TIME-RESOLVED FLUORESCENCE WITH SUBNANOSECOND RESOLUTION.
B. Feddersen, E. Gratton, R. M. Clegg* and T. Jovin.* *Laboratory for Fluorescence Dynamics, University of Illinois at Urbana-Champaign, 1110 W. Green Street, Urbana, IL 61801 and *Max-Planck-Institut für biophysikalische Chemie Karl-Friedrich-Bonhoeffer-Institut Göttingen-Nikolausberg, Germany.*

Area detectors such as diode arrays and CCD cameras have been employed in frequency domain fluorometry with subnanosecond resolution. The crucial component is a modulated image intensifier in front of the detector which down converts the high frequencies to a lower frequency which can be handled by the array detector. However, some array devices have a very slow reading frame, on the order of seconds or longer. A single step frequency conversion to the very low frequencies (DC to 1Hz) needed by these detectors is either very expensive or impossible. We have developed a method which uses a two-step frequency conversion to avoid this problem. In the first step the modulation capabilities of the intensifier are used to convert from high frequency (generally 10-100MHz) to an intermediate frequency on the order of 10-500Hz, just as before. This step is done electronically. A second conversion step translates the intermediate frequency down to very low frequency, DC to 1Hz. The second step is done optically by using a chopper in the light beam to provide an optical heterodyning signal. The frequency of the chopper is controlled by a source which is phase locked to the intermediate frequency. This scheme has been successfully applied to a diode array detector and other array devices, and it can find a general application to frequency-domain spectroscopy. (Supported by NIH grant RR03155).

M-Pos406

SIMULTANEOUS FLUORESCENT AND TRANSMISSION LASER SCANNING CONFOCAL MICROSCOPY.
JJ Art, MB Goodman, EA Schwartz. (Intro. by R Rogart)

Enhanced fluorescent images of ion-concentration and membrane potential in living cells can be obtained using the optical sectioning inherent in laser scanning confocal microscopy (LSCM). Radiation damage to the tissue can be minimized and the sensitivity of the optical measurement maintained by increasing the probability of photon detection. Methods are presented that double the probability of detection of emitted photons, and simultaneously produce a true transmission confocal image with either brightfield or differential interference contrast (DIC).

In this technique the usual microscope condenser is replaced by a secondary microscope objective and plane mirror. These elements are positioned so that light passing through the object is focused back to the same point as the incident beam. The advantages of this method over conventional LSCM configurations are at least twofold.

First, the solid angle in which fluorescent photons may be captured is effectively doubled. In particular, complex living tissue may require the use of an upright microscope and long working distance, low numercial aperture (NA), water immersion objectives (e.g. Zeiss X40/0.75 NA). Addition of an identical substage objective and mirror permits photon capture over a solid angle of 2.14 steradians. This approaches the 2.75 steradians that can be achieved with oil-immersion high NA objectives. Use of a water immersion objective and mirror as a reflecting condenser on an inverted microscope increases the solid angle of capture by 39% to 3.79 steradians over that produced by a 1.4 NA objective alone.

Second, this technique produces a true confocal transmission image without the use of additional scanning elements. With DIC the image is further enhanced by a doubling of the optical path length.

For both fluorescent and transmission micrscopy the specimen is an an optical element in the detection path. To maintain confocality between the illumination and detection, the primary and secondary objectives are focused in tandem. To further optimize detection, the secondary detector is micropositioned under servo control.

This work supported by: DC00454-03 (NIH), N00014-88 (ONR) and A.P. Sloan Fellowship to JJA; Howard Hughes Predoctoral Fellowship to MBG; EY02440-12 (NIH) to EAS; and Brain Research Foundation grant to JJA & EAS.

**M-Pos407**

## BACKGROUND REJECTION IN FLUORESCENCE CONFOCAL MICROSCOPY

*D. R. Sandison*, W. W.Webb, School of Applied and Engineering Physics and Department of Physics*, Cornell University , Ithaca NY*

The hallmark of successful confocal microscopy is a crisp image of an optically thin section deep within a thick sample. This has little to do with the improved lateral or longitudinal resolution of the confocal microscope because the gain in resolution is at best a factor of two. We show that the confocal sectioning capability is a result of background rejection two orders of magnitude greater than that of a conventional microscope as measured by the signal-to-background ratio. To evaluate instrument design, we have analyzed background rejection as a function of sample thickness for various illumination schemes. We calculate the following approximate signal-to-background ratios for a thick sample with a point detector: widefield illumination 0.06, line illumination 0.6, spinning disk (1% hole coverage) 0.8, single spot confocal 4.2, two-photon illumination (infinite detector aperture) 4.2, two-photon confocal 120. The signal-to-background ratio is maximum for a point detector but is not an appropriate measure of image quality since shot noise must be taken into account. Background photons contribute to shot noise in the image so the noise limit on imaging speed is different for each illumination method. We have calculated the optimal detector aperture radius by maximizing the signal-to-noise ratio, a quantitative measure of image quality.

Supported by the Developmental Resource for Biological Imaging and Opto-electronics funded by the NIH(5P41RR04224) and NSF(DIR-8800278).

**M-Pos408**

## Comparison of Optical Sectioning by Confocal Microscopy(LSCM) and Widefield Image Processing

*L.P. Ghislain* and W.W. Webb, School of Applied and Engineering Physics and Department of Physics*, Cornell U, Ithaca N.Y.*

Confocal imaging improves axial resolution and background rejection to provide clear optical sections by use of focussed illumination and spatially filtered detection. It is also possible to produce clear optical sections by widefield microscopy with the help of image processing; the Nearest Neighbour Deblurring(NND) algorithm (Agard *etal.* (1988) Meth. Cell Biol. 30:353) uses the information in 3 images of a 3-D specimen taken at $z_o$ and $z_o \pm \Delta z$ to remove out of focus contributions. We aim to compare the performance of LSCM and widefield NND sectioning by application to test samples composed of 3-D dispersed fluorescent point sources in a dark background and unlabelled microspheres suspended in a uniform fluorescent background gel in order to evaluate resolution and background rejection. The unlabelled beads have been predicted to vanish into background at a threshold radius that is smaller in LSCM than widefield. The NND reconstruction algorithm improves resolution and reduces background but not noise levels whereas the confocal detector aperture reduces background and noise levels by reducing out of focus shot noise contributions.

Supported by the Developmental Resource for Biological Imaging and Optoelectronics funded by the NIH (5P41-RRO-4224) and NSF(DIR-8800278).

**M-Pos409**

## THREE DIMENSIONAL IMAGING OF INTRACELLULAR CALCIUM ACTIVITY, USING TWO-PHOTON EXCITATION OF THE FLUORESCENT INDICATOR DYE INDO-1 IN LASER SCANNING MICROSCOPY

*David W. Piston and Watt W. Webb, School of Applied and Engineering Physics, Cornell University, Ithaca, NY 14853.*

Two-photon excitation of fluorescence in laser scanning microscopy provides imaging of ultraviolet excitable fluorophores without exposure to UV wavelengths. Application of two-photon excitation to Indo-1 makes possible the recording of three dimensional intracellular free calcium concentration distributions. In our apparatus, 100fsec pulses of 700nm laser light, generated at 80MHz by a Coherent Satori dye laser, are scanned through the cells by a Biorad MRC-600 confocal scanner. Due to the quadratic intensity dependence of absorption in the two-photon process, the resulting excitation is limited to the focal volume, and thus fluorescence and photobleaching are limited to the focal plane during the imaging scan. The pinhole, ordinarily used as a spatial filter in confocal microscopy, is not needed to obtain depth resolution. Instead, the fluorescence signal is split by a dichroic mirror into the emission peak of the calcium bound fluorophore ($\sim 405nm$) and the calcium free peak ($\sim 485nm$), and monitored simultaneously by two detection channels placed at a plane conjugate with the back aperture of the objective. Intracellular free calcium is imaged using the calibrated ratios of these two intensities. The calibration is determined from measured intensity ratios at several calcium concentrations as a function of excitation parameters. The two-photon bleaching rate for Indo-1 is being determined in vitro. Measurements of second messenger calcium activity due to cell surface receptor stimulation are currently underway. Supported by the Developmental Resource for Biological Imaging and Opto-Electronics (NIH 5P41-RR-04224 and NSF DIR-8800278).

**M-Pos410**

## RATIO IMAGING OF EMISSION SHIFT FLUORESCENT INDICATORS.

John S. George, Biophysics Group , Los Alamos National Laboratory, MS: M-715, Los Alamos, NM 87545

We have previously reported the use of an intensified video camera to image patterns of neural population activity in the mammalian hippocampal slice [1]. The fluorescent $Ca^{2+}$ indicator Fura-2 was loaded into cells in the slice by incubation, and a difference image ratio was computed to visualize the spatial and temporal pattern of the fluorescence transient associated with electrical excitation of the tissue. This approach requires summation of a large number of image sequences due to the small size of the signal and the noise generated by operating the intensifier near maximum gain. In principle, indicators such as Indo-1, which respond with an emission shift may have significant advantages for these experiments. However, practical considerations such as the cost of paired intensified video cameras or cooled CCD imagers with the requisite sensitivity have limited such applications. We have designed and fabricated an optical system for simultaneously collecting dual wavelength images using a single camera. The image is split using an optical assembly analogous to a microscope binocular head. Image paths are filtered separately, and recombined into a side by side image using a system of prisms. Image processing software allows ratioing of subregions within each frame of a video time sequence. The system should provide better control of experimental variables such as lamp fluctuation, changes in intensifier response characteristics, or changes in optical properties of the preparation. The use of emisson shift indicators should facilitate increased fluorescence intensity by using a broader excitation band and/or using a single spectral line from a mercury arc lamp rather than selecting multiple bands from the spectrally flatter but less intense xenon source.

1. J.S. George, J.C. Fowler and D.M. Ranken, Biophys J., 57:131a (1990)

**M-Pos411**

3D microscopic analysis of hexokinase distribution in vivo. R.M. Lynch, K.E. Fogarty W. Carrington and F.S. Fay, Univ. Mass. Med. Ctr, Worcester, MA 01655.

In order to understand the dynamics of association of cytoplasmic hexokinase I (HK) with mitochondria (Mito) in living cells, we analyzed distributions of carboxyrhodamine-X labeled HK (X-HK) relative to fluorescein dextran (F-Dex). The probes were microinjected into living A7R5 smooth muscle cells. Distributions of fluorescent molecules were evaluated using a Zeiss IM-35 microscope equipped with a Photometrics CCD camera. After injection, HK becomes localized to Mito. On the other hand, F-Dex remains distributed through out the cell. X-HK localization in discrete subcellular regions was analyzed by acquiring a series of optical sections and then reconstructing the underlying molecular distribution. Since significant photobleaching occurs with repetitive imaging, limited data (7 planes) were acquired symmetrically about the plane of interest. An algorithm based on regularization with a non-negativity constraint was used to restore data in the primary plane of focus (J. Microsc. 153:133, 1989). After restoration, the ratio between X-HK and F-Dex were computed for various subcellular regions. Images were acquired within 5 min after injection, and then at 10 min intervals for up to 1 hour. The amount of HK associated with individual Mito relative to cytosolic regions increased with time after injection until a steady state was reached. In initial studies inhibition of glycolysis with 2-deoxy glucose lead to a significant decrease in Mito localized HK relative to cytosolic HK. The results indicate that the distribution of HK is dynamically regulated in the intact cell. This approach should allow for a detailed characterization of the mechanisms of the association of hexokinase with Mito under a wide range of conditions in living cells.

**M-Pos412**

QUANTITATIVE MAPPING OF INTEGRATED HUMAN PAPILLOMA VIRUS ON HUMAN METAPHASE CHROMOSOMES USING A FLUORESCENCE MICROSCOPE IMAGING SYSTEM . D.E. Callahan, A. Karim, G. Zheng, P.O.P Ts'o and S.A. Lesko, Department of Biochemistry, School of Public Health, The Johns Hopkins University, 615 N. Wolfe Street, Baltimore, Maryland 21205.

Previous studies of the SiHa and CaSki cervical carcinoma cell lines have used filter hybridization and radioactive probes to quantitate the amount of integrated human papilloma virus type 16 (HPV-16) in the cells and to map the integration site in SiHa cells to a region between q14 and q32 on chromosome 13. These studies have indicated that SiHa cells contain 1-2 copies of HPV-16, while CaSki cells contain greater than 500 copies. We have attempted to verify these results using in situ hybridization and a fluorescence microscope imaging system . A biotinylated HPV-16 DNA probe (7.9-kb) was detected using an amplified avidin-FITC detection system. FITC fluorescence signals were imaged using a cooled-CCD camera interfaced to an image processor and host computer, and were localized on specific chromosomes using separate, registered images of isolated, DAPI or propidium iodide stained metaphase chromosome spreads. Simultaneous hybridizations using a biotinylated centromere probe specific for chromosomes 13 and 21 were also performed. In both SiHa and CaSki spreads, a single fluorescent signal could be observed on one or both chromatids of chromosome 13. Ratios of the distance from 13pter to the signal to the total chromosome length were approximately 0.63±8%, corresponding to the region between 13q21.31 and 13q22.3. This confirms the results of previous mapping studies, and is also an improvement in resolution. The mean intensity of these single fluorescent signals was normalized to the mean intensity of a standard at an equivalent exposure time, and the total integrated intensity was obtained. No additional signals were observed in SiHa chromosomes, suggesting that each single signal on chromosome 13 represents one equivalent of HPV-16 genome. The total integrated intensity in CaSki spreads was approximately two orders of magnitude greater than that observed in SiHa spreads, confirming that CaSki cells contain hundreds of copies of HPV-16. Approximately 90% of the fluorescence observed in CaSki spreads was highly localized in 6-8 small clusters, and was located on chromosomes other than chromosome 13. These results illustrate the applicability of the current imaging system to gene mapping, ordering of contigs along metaphase chromosomes for sequence analysis, and studies of nuclear topography. (Supported in part by DOE and NIH).

**M-Pos413**

CHANGES IN ADHESION PATTERNS OF RAT MESOTHELIOMA CELLS INDUCED BY ASBESTOS. M. Lee, S. Schürch, and F. Green, Departments of Medical Physiology and Pathology, University of Calgary, Calgary, Alberta, Canada.

Mesothelioma is a malignant neoplasm that arises from the serosal lining of the lungs and peritoneal cavity. Mesotheliomas were induced in Fischer 344 rats following intraperitoneal injection of crocidolite asbestos. Cultured mesothelioma cells manifested both sarcomatous (SM) and epitheliomatous (EM) phenotypes. The SM cells demonstrated adherence to clean glass and readily grew to confluence in vitro; whereas, the EM cells remained in suspension. The morphology of the SM cells is spindle shaped and formed lamellipodia from which small filopodia protrude radially outward. In contrast, the EM cells showed a roundly shaped geometry and tend to aggregate. We used Interference Reflection Microscopy (IRM) to study the adhesion patterns of these two phenotypes of mesothelioma cells after 48 hours of incubation on clean coverglass. Adhesion was defined by the number of video pixels of cell area in which the grey level is greater than six standard deviations of the background grey level. The mean pixel count per video frame for the SM cells was 1163 ± 307 SE while the mean for the EM cells was 22 ± 22 SE. The total IRM area was also measured. The mean for the SM cells was 24552 ± 4672 SE square pixels and the mean for the EM cells was 17914 ± 2,112 SE square pixels. Most of the adhesion for the SM cells occurred near the lamellipodia region. These surface property changes was correlated with contact angle measurements using a two phase aqueous polymer system containing 4% Dextran (MW $2 \times 10^6$) and 4% PEG (MW 20000).

**M-Pos414**

**THREE-DIMENSIONAL VISUALIZATION OF THE LIVING EYE.**

Barry R. Masters, Georgia Institute of Technology, School of Electrical Engineering, Atlanta, Georgia 30332-0250

The three-dimensional reconstruction of the optic zone of the cornea and the ocular crystalline lens has been accomplished using confocal microscopy and volume rendering computer techniques. A laser scanning confocal microscope was used in the reflected light mode to obtain the two-dimensional images from the cornea and the ocular lens of a freshly enucleated rabbit eye. The light source was an argon ion laser with a 488 nm wavelength. The microscope objective was a Leitz X25, NA 0.6 water immersion lens. The 400 micron thick cornea was optically sectioned into 133, three micron sections. The semi-transparent cornea and the in-situ ocular lens was visualized as high resolution, high contrast two-dimensional images. The structures observed in the cornea include: superficial epithelial cells and their nuclei, basal epithelial cells and their "beaded" cell borders, basal lamina, nerve plexus, nerve fibers, nuclei of stromal keratocytes, and endothelial cells. The structures observed in the in-situ ocular lens include: lens capsule, lens epithelial cells, and individual lens fibers. The three-dimensional data sets of the cornea and the ocular lens were reconstructed in the computer using volume rendering techniques. Stero pairs were also created of the two-dimensional ocular images for visualization. This demonstration of the three-dimensional visualization of the intact, enucleated eye provides an important step towards quantitative three-dimensional morphometry of the eye. Support from N.I.H. EY-06958.

**M-Pos415**

EIGENANALYSIS OF DIGITAL IMAGES IN THE FOURIER DOMAIN: A STUDY OF HIGH RESOLUTION HUMAN CHROMOSOMES. Z. Jericevic, L.C. Smith and L. McGavran, Baylor College of Medicine, The Methodist Hospital, Houston, Texas 77030, and The Children's Hospital, Denver, Colorado 80218-1088.

Eigenanalysis is a mathematical approach used to obtain characteristic roots and vectors from a matrix and is an important method for extracting information from digital images in microscopy. To use multiple images as input data, the images must be correctly aligned and the pattern common for each input image must not be geometrically distorted. Otherwise, the different geometries produce blurring. Alignment and removal of geometric distortion of 40 digital images of random examples of high resolution preparations of human chromosomes as a data set has been achieved using the phase synchronization approach in which eigenanalysis is performed in the Fourier spectral domain on the phase and the amplitude of the Fourier transform. Our results show that eigenanalysis in the frequency domain provides a better resolution of features then does eigenanalysis in the spatial domain. After the eigenanalysis further improvement of images is achieved by the iterative Fourier synthesis using an iterative phase synthesis similar to that used in crystallography.

M-Pos416

## OPTIMIZATION OF THE MAXIMUM LIKELIHOOD METHOD FOR FLUORESCENCE INTENSITY DECAY ANALYSIS

**Ž. Bajzer, P.H. Axelsen, T.M. Therneau, and F.G. Prendergast**
**Mayo Clinic and Foundation, Rochester, MN, 55905**

**The measurement of fluorescence intensity decays by time-correlated single photon counting can now be performed with an unprecedented degree of precision. This precision allows and demands that more sophisticated methods be applied to data analysis. We have recently shown (Biophys J. 57:190a,1990) that the maximum likelihood (ML) method is generally more accurate than the standard least-squares method for such analysis. We now propose two improvements within the framework of the ML approach: 1) elimination of systematic error due to light scattering, and 2) optimization of analysis by combining measurements with different channel widths, using statistical methods for design of experiments.**

**These improvements offer advantages when a very short lifetime is present or the when two similar discrete lifetime components are present. In addition we compare 3 different discretization schemes for the convolution integral in order to find the most successful scheme for the case of short lifetimes. The optimized method is illustrated by an analysis of fluorescence lifetimes in mutated forms of glutamine binding protein from E. coli.**

**Supported by GM 34847.**

M-Pos417

## APPLICATION OF SINGULAR VALUE DECOMPOSITION TO THE ANALYSIS OF EXPERIMENTAL DATA.

Eric R. Henry and James Hofrichter, Laboratory of Chemical Physics, NIDDK, NIH, Bethesda, Maryland 20892.

Singular value decomposition (SVD) is a powerful tool for processing large matrices of experimental data. The SVD of a m×n matrix A may be written as the product $A = U S V^T$, where U is a m×n matrix of orthonormal basis vectors, S is a n×n diagonal matrix with non-negative diagonal elements which are called the singular values of A, and V is a n×n matrix of orthonormal amplitude vectors. The columns of U and V corresponding to the r largest singular values provide the optimal least-squares approximation to A having rank r. A minimal description of an experimental data matrix which is correct to within experimental error may usually be constructed from a small number of components produced by the SVD, effecting a significant reduction in the number of parameters required to describe a data set. We have extensively studied the properties of the SVD of matrices in the presence of measurement noise. The effects of various types of noise on the SVD may be determined analytically in certain special cases, and by statistical simulations of large ensembles of matrices in general. We have developed a procedure for optimizing the signal-to-noise of basis or amplitude vectors constructed as linear combinations of a chosen set of SVD components. We have also developed a general procedure for optimal statistical weighting of the various elements $A_{ij}$ of the data matrix prior to SVD, based upon the known variances $\sigma_{ij}^2$ of all of the elements. SVD-based analysis of data sets measured as a function of several experimental variables will be discussed, as well as the use of SVD combined with least-squares fitting to analyze data matrices in terms of physical models.

M-Pos418

## A NEW METHOD FOR BACKGROUND SUBTRACTION IN FREQUENCY-DOMAIN FLUORIMETRY.

*Kerry Swift, George Mitchell, Michael Armijo and A.S. Verkman. SLM Instruments Inc. and U.C.S.F.*

Fluorescence experiments on biological systems are often complicated by the presence of a large background signal from autofluorescence and/or excitation scattering. To date, correction of these artifacts in frequency domain fluorimetry has required frequency-by-frequency phase/modulation measurements on a suitable blank followed by vector subtraction of blank values from sample values (Lakowicz et al, Anal. Biochem. 160:471, 1987). A new form of phase fluorimeter uses the Fourier transform to extract multi-harmonic phase and modulation values from digitized time domain waveforms (Mitchell and Swift, Proc. SPIE 1204:270, 1990). Time domain data for a blank may be time-justified and subtracted directly before transformation of experimental results to the frequency domain. This approach yields excellent correction over a wide dynamic range of background intensities and decay patterns and is more intuitive than the vector subtraction approach. The new methodology was validated by experiments on standard fluorophores in cuvettes and in living cultured cells studied by epifluorescence microscopy. In cuvettes, fluorescence of 1 uM fluorescein in 0.1 M NaOH (lifetime 3.8 ns) was excited at 488 nm in the presence of the "background" compounds acridine orange (lifetime 2.2 ns) or glycogen. Background fluorescence in the steady-state was adjusted to be 0-90% of total fluorescence. The recovered fluorescein lifetime in the background-corrected samples was in the range 3.7-4.0 ns for background intensities from 0 to >80% of total intensity. For cell studies, Swiss 3T3 fibroblasts were loaded with the pH indicator BCECF, mounted in a perfusion chamber, and illuminated with the modulated focused laser beam (1 micron dia) through a 40x quartz objective (glycerol immersion, N.A. 0.65). A single lifetime (4.2 ns) was detected in the presence of a heterogeneous background signal making up >50% of total signal. These results establish and validate a direct approach for subtraction of background fluorescence in frequency domain fluorimetry.

M-Pos419

## $^{12}C/^{13}C$ MEASUREMENTS USING TUNABLE DIODE LASER SPECTROSCOPY.

Todd B. Sauke, Solar System Exploration Branch, NASA Ames Research Center, Joseph F. Becker, Thomas Gutierrez, Vincent Dinh, Physics Dept., San Jose State U.---Stable isotopic ratio measurements are used in such diverse fields as medical diagnostics, petroleum prospecting, and planetary exploration. Laser spectroscopy offers important advantages over conventional mass spectrometry for *in situ* measurements. The complex and detailed sample preparation and purification necessary for reliable mass spectrometer measurements are unnecessary when a laser spectrometer is used because foreign gases and pyrolysis products do not interfere with the measurement. Lead-salt tunable diode lasers (TDL) emit with a very narrow linewidth of approximately 0.0003 $cm^{-1}$. It is thus possible to resolve individual rotational lines within the vibrational band and measure their intensity, which can be used to determine gas concentration and isotopic ratio. The 2300 $cm^{-1}$ spectral region is especially interesting because the $^{12}CO_2$ and $^{13}CO_2$ bands overlap in such a way that their rotational lines have approximately equal absorbance at the normal isotopic ratio (~89) of $CO_2$. Rotational lines we have studied are separated by as little as 0.050 $cm^{-1}$ but are well resolved using a TDL. Using sophisticated sweep integration and signal averaging techniques, we have measured the stable isotopic ratio of carbon in carbon dioxide to an accuracy of better than 0.4%. With the improvements in the data acquisition and analysis systems presently underway in our laboratory we expect to attain an accuracy of better than 0.1%. Supported in part by NASA NCA2-407 and NSF-REU PHY-9000697; this work was done while one of the authors (TBS) held a National Research Council-NASA ARC Research Associateship.

**M-Pos420**

**DETECTION OF RADIOLUMINESCENCE FROM TRITIUM DECAY BY SINGLE PHOTON COUNTING: EVALUATION AS A MOLECULAR RULER.** *Zahra Shahrokh, Stephen B. Shohet, and A.S. Verkman. University of California, San Francisco.*

Determination of molecular dimensions by radioluminescence provides a novel approach to extend the ~80 Å distance limit measurable by fluorescence energy transfer. The radioluminescence signal depends on the inverse square of the distance between a radioactive "donor" and a fluorescent "acceptor" (Radda et al BBA 601:63, 1980), allowing distance determinations of up to 500 Å for $^3$H as the donor. To measure the single photon radioluminescence signal, light from 0.5 ml samples was detected by a cooled photomultiplier using efficient light collection optics. Signal-to-noise ratio was maximized by detection of a differential signal in the gated mode using an optical chopper between the sample and the photomultiplier. At the gain and discriminator levels required for signal detection, <10 counts per second (cps) was measured in the absence of sample. Signals less than 0.5 cps above background could be measured with 30 min data accumulation. Experiments were carried out using $^3$H-palmitic acid ($^3$H-PA) as the donor and 12-(9-anthroxyloxy) stearic acid (9-AS) as the acceptor. The background-subtracted signal from micelles containing 1.7 μM $^3$H-PA (90 μCi/ml) and 10.5 μM 9-AS was 236 ± 15 cps (S.D.), compared to 18 ± 5 cps for $^3$H-PA alone. The signal from 9-AS alone was the same as background. The signal from sonicated unilamellar vesicles (200 Å diameter) prepared from 200 μM phosphatidylcholine and the same probe concentrations as above was 16 ± 7 cps with 30 min accumulation time, compared to 1 ± 3 cps for vesicles containing $^3$H-PA alone. For the same surface density of $^3$H-PA and 9-AS, the signal from the sonicated vesicles did not differ significantly from the signal from 10-fold larger vesicles prepared by the extrusion method (14 ± 5 cps). The smaller radioluminescence signal in the bilayer vesicles compared to micelles is consistent with the increased donor-acceptor distance associated with their dilution by the phosphatidylcholine. Thus, this study establishes a sensitive method for the detection of single photon radioluminescence which has potential application to the determination of long-range tritium-fluorophore distances in biological membranes.

**M-Pos421**

**A COMPUTER MODEL FOR PHOTON MIGRATION IN TURBID MEDIA.** **C. Yee, G. Herman, and B. Chance, U. of Penn., Phila., PA 119104**

A computer based discrete diffusion model has been developed which is capable of simulating the migration of visible or near-infrared photons in a turbid media. Such photons are highly scattered and soon lose any directionality they may have had on injection. The model is capable of predicting the distribution of the photons exiting the media given information concerning the scattering and absorption properties of the media.

The model divides the media into cubic voxels. The scattering and absorption properties of the media is assumed to be uniform within each voxel but may vary between voxels. Photons within a voxel are able to move to adjacent voxels, stay within the voxel or be absorbed. The probability of each of these events is dependant upon the scattering and absorption properties of the media. Photons which escape the media are recorded by the model at each point on the surface as a function of time.

Since the problem is computationally very expensive and highly parallel in nature, an AT&T Pixel Machine was chosen to implement the algorithm. The Pixel Machine is an 82 processor computer in which 64 of its processors are arranged in an 8x8 array while the remaining are arranged as a pipeline. Thus, each processor in the array can be responsible for a contiguous column of voxels in the model.

Initial results from this model compare favorably with the results of Patterson et. al.[1] and Bonner et. al.[2] which state that at times far from the initial injection point, the rate of decay of the photon intensity is exponential and is dependent upon the absorption coefficient of the media.

[1] M. Patterson, B. Chance, and B. Wilson. Time resolved reflectance and transmittance for the non-invasive measurement of tissue optical properties. *Applied Optics*, 28:2331–2336, 1989.

[2] R. Bonner, R. Nossal, S. Havlin, and G. Weiss. Model for photon migration in turbid biological media. *Journal of the Optical Society of America A*, 4:423–432, 1987.

**M-Pos422**

QUANTITATION OF TISSUE OXYGENATION USING DUAL-WAVELENGTH PHASE MODULATED SPECTROSCOPY. E.M. Sevick and B. Chance, Department of Biochemistry and Biophysics, University of Pennsylvania, Philadelphia, PA 19104-6089.

We have previously demonstrated the utility of phase-modulated spectroscopy to quantitate the absorption coefficient, $\mu_a$ ($cm^{-1}$), in a highly scattering medium (1). Herein, we have employed dual-wavelength reflectance measurements of phase-shift, θ, at 754 and 840 nm at 200 MHz to demonstrate the use of phase-modulated spectroscopy to quantitate hemoglobin saturation in media which simulate the optical properties of tissue.

Reflectance measurements of phase-shift, θ, were made on a closed, *in vitro* model of 0.5% intralipid and 1% yeast with 10-50 μM hemoglobin added to simulate the optical and hemoglobin absorption properties of tissue. Measurements of phase-shift in the absence and presence of hemoglobin were made at the two wavelengths as well as during hemoglobin deoxygenation ($pO_2$ 200 --> 0 mm Hg) due to the respiration of yeast. Controlled reoxygenation was performed by oxygen transfer from silastic tubing.

Using the Fourier transform of the diffusion approximation to predict phase-shift as a function of $\mu_a$ (1), one can show that the ratio of θ in the presence of hemoglobin relative to that due to scattering ($\theta_o$) is equal to the ratio of absorption coefficients {i.e. $(\theta - \theta_o)^{754}/(\theta - \theta_o)^{840} = \mu_a^{754}/\mu_a^{840}$}. Since the two wavelengths straddle the hemoglobin isosbestic point (800 nm), $\mu_a^{754}/\mu_a^{840}$ is a unique and sensitive function of hemoglobin saturation. Thus, hemoglobin saturation can be predicted from measurements of θ independently of the total hemoglobin concentration.

Our results demonstrate that the ratio of phase-shifts measured at 754 and 840 nm at 200 MHz accurately monitors solution $pO_2$ in equilibrium with hemoglobin. The use of this technique and algorithm has been successfully applied to determine tissue oxygenation in brain, skeletal muscle, and tumor.

[Supported by NIM, Inc., NIH CA08783, NS-27346, and HL 44125]

(1) M.S. Patterson, J.D. Moulton, B.C. Wilson, and B. Chance. Applications of time-resolved light scattering measurements to photodynamic therapy dosimetry, SPIE (J. Appl. Optics) in press.
(2) B. Chance and E.M. Sevick. Correlation of time and frequency domain measurements of hemoglobin absorbance changes in tissue models, (this volume).

**M-Pos423**

IN VIVO TIME RESOLVED SPECTROSCOPOY OF HUMAN BRAIN. Michael Maris, Nai Guang Wang, Weija Cui, Scott Williams* & Britton Chance. Department of Biochemistry & Biophysics and *Chemistry, University of Pennsylvania, Philadelphia, PA 19104

Time Resolved Spectroscopy (TRS) measurements of photon migration of light in the red and near infrared (600-800nm) were made on several adult subjects. A mode-locked Coherent YAG laser pumped a cavity dumped dye laser produced 6ps pulses that were brought via fiber optics to the subjects forehead. Another fiber optic collected light at a 3cm separation and brought it to a Hamamatsu microchannel plate detector. Standard time correlated single photon counting techniques were used. The dyes used for the study were Rhodamine-6G, LDS-698, and LDS-751 which permitted selecting wavelengths at 10 nm intervals between 600 nm and 800 nm. Our results show i) a characteristic time delay between incident light and detected light ii) a rapid rise to broadened peak which decays exponentially iii) an increase in absorption as the wavelengths drop below 690 nm iv) an absorption peak at 760 nm for deoxyhemoglobin was resolved. The absorption coefficient ($\mu_a$) was calculated by measuring the slope of the exponential decay (intensity vs time) and dividing by the speed of light in water. Hemoglobin saturation was calculated from the ratios of the absorption coefficients at appropriate wavelengths. TRS allows non-invasive and quantitative in vivo determination of tissue oxygenation status.

This work was supported by NIH grants NS-27346, HL-44125 & NIM inc.

M-Pos424

## INVESTIGATION OF COMPLEX SPECTRAL CHARACTERISTICS OF MONOVINYL PROTOPHEOPHORBIDE BY FREQUENCY DOMAIN TIME-RESOLVED METHODS.

James R. Mattheis. *Laboratory for Fluorescence Dynamics, University of Illinois at Urbana-Champaign, 1110 W. Green Street, Urbana, IL 61801.*

The tetrapyrrole monovinyl protopheophorbide is a member of the class of important biomolecules called phorbins and is derived from a precursor of chlorophyll *a*. This molecule exhibits unexpectedly complex electronic spectral characteristics not observed in more symmetric porphyrins such as protoporphyrin IX or in the metallated form, monovinyl protochlorophyllide. The complexity is seen as a split in the emission band with the proportions of the two bands dependent upon both the excitation wavelength and temperature.

Recent advances in frequency domain time-resolved fluorescence methods and the possibility of millisecond kinetics of time-resolved fluorescence have enabled a more detailed investigation into this spectral complexity and the possible role of N-H tautomcism.

M-Pos425

## LUMINESCENCE PROPERTIES OF LANTHANIDE COMPLEXES WITH 4-SUBSTITUTED DIPICOLINIC ACID ANALOGUES

Jagannath B. Lamture, Zhenghong Zhou, A. Suresh Kumar and Theodore G. Wensel *Department of Biochemistry, Baylor College of Medicine, One Baylor Plaza, Houston, TX 77030*

Energy transfer from dipicolinic acid and its analogues to bound Tb(III) or Eu(III) results in dramatically enhanced luminescence from the bound lanthanide ions. Because of their large Stokes shifts and millisecond-range excited state lifetimes, such complexes are very useful in energy transfer studies of biological systems, and in delayed luminescence immunoassays. The greatest limitations to their use have been: a requirement for excitation at wavelengths $\leq$ 280 nm, weak binding, and lack of analogues suitable for attachment to macromolecules. To develop analogues with more useful properties, we have prepared a series of Tb(III) and Eu(III) complexes with compounds of the type 4-X -dipicolinic acid, where X is -H, -OH, -Cl, -Br, $-NH_2$, or $-NHOCCH_3$, and compared their spectral properties, including absorbance, excitation and emission spectra, and luminescence lifetimes. At excitation wavelengths > 294 nm, the most efficient energy donor to Tb(III) is 4-amino dipicolinic acid. The most efficient donor at wavelengths < 294 nm is the 4-acetamido derivative. When -Br is substituted for -Cl at the 4 position, there is no enhancement of energy transfer due to heavy atom effects on inner-system crossing. All the Tb(III) complexes display single lifetimes in the millisecond range. Supported by the Whitaker Foundation, the Welch Foundation, and the Texas Advanced Technology Program.

M-Pos426

## INVESTIGATIONS OF COBALAMIN REACTIVITY USING CRYOGENIC OPTICAL SPECTROSCOPY

*E. Chen and M.R. Chance, Department of Chemistry, Georgetown University, Washington, DC 20057.*

The absorption spectrum of cobalamins reflect the $\pi$-$\pi^*$ transitions of the corrin ring chromophore. At low temperatures the vibrational modes of these spectra are enhanced. Changes in the optical spectrum are due primarily to the effect of the axial ligand on the electron density of the corrin ring (Firth et al., *Biochem.*, 6, 1967, p. 2178). Therefore, cyrogenic optical spectroscopy studies with different $B_{12}$ compounds and different solvents may be used to distinguish charge transfer, metal-metal and metal-ligand transitions that may also be present. This will lead to better understanding of the electronic and/or conformational changes resulting from interaction of $B_{12}$ dependent enzymes with the corrin ring amide side chains of cobala-mins that lead to homolytic cleavage of the Co-C bond.

A 1-5 progression of 1185 $cm^{-1}$ from the lowest energy peak is observed for coenzyme $B_{12}$ in phenol. Coenzyme $B_{12}$ in water exhibits a similar 1-5 progression of 1185 $cm^{-1}$, however, the third overtone is missing. Photolyzed coenzyme $B_{12}$ shows an overtone of 1080 $cm^{-1}$ in phenol and water solvents. In both solvents photolyzed coenzyme $B_{12}$ exhibits similar 1-4,6 progressions, however, in phenol the third overtone is also missing. These results suggest the presence of charge transfer, metal-ligand, or metal-metal transitions. Charge transfer transitions are strongly suggested by dramatic changes in the optical spectrum of coenzyme in phenol *vs.* water. Recent FTIR studies (Chen, et al., *this meeting.*) have shown that Pt(II) interaction at the corrin ring amide side chains of methylcobalamin ($MeB_{12}$) to form a Pt(II)-$MeB_{12}$ complex results in increased reactivity through labilization of the sixth axial ligand. The nature of the interaction of Pt(II) and protein with the amide side chains, along with metal free corrinoids will be examined to determine which transitions are influenced.

This research is supported by CSRS U.S. Department of Agriculture under grant #90-37200-5357 of the Program in Human Nutrition.

M-Pos427

## COMPARATIVE FLUORESCENCE SPECTRA FROM BACTERIA AND SPORES IN DIFFERENT STAGES OF GROWTH.

L. Reinisch*, W.P. Van De Merwe*, and B.V. Bronk†

** Uniformed Services University of the Health Sciences, Bethesda, MD 20814 and † U.S. Army Chemical Research Development and Engineering Center, APG, Maryland 21010*

Several species of bacteria and bacterial spores were studied with fluorescence excitation and emission spectroscopy. With dilute room temperature suspensions, we have found reproducible characteristics in the fluorescence spectra from several different species of bacteria. These characteristics are independent of the conditions of growth and may be useful as a means of rapid species identification. In general, the excitation spectra peak near 280 nm with a peak near 340 nm for the emission spectra. A broader emission spectrum is obtained from the spores in comparison to the emission spectrum from the bacteria. When *B. Megaterium* spores are stimulated to germinate, the changes from spores to bacteria can be monitored in the fluorescence spectra. Additional information, available from polarized "elastic" light scattering, can be used to augment the species identification.

**M-Pos428**

ULTRAVIOLET LINEAR DICHROISM STUDY OF THE DNA STRUCTURES IN FOUR FILAMENTOUS BACTERIOPHAGES: FD, IKE, PF1, AND PF3. B. A. Clack and D. M. Gray, Program in Molecular and Cell Biology, University of Texas at Dallas, Richardson, TX, 75083-0688.

Linear dichroism (LD) spectroscopy measurements provide information on the orientation of transition moments within oriented biological macromolecules. We have utilized this technique to investigate the structure of the single-stranded DNA packaged within four filamentous bacteriophages: fd, IKe, Pf1, and Pf3. We report the intrinsic LD of each flow-oriented phage from 310 nm to 190 nm. The DNA and protein contributions to the LD were separated and the maximum angle of tilt of the DNA bases relative to the helix axis (long axis of the phage) was determined for each phage. For the class I phages, fd and IKe, the maximum average angles of base tilt were 63° and 64°, respectively. For the class II phages, Pf1 and Pf3, the angles of base tilt were 51° and 49°, respectively. Thus, the DNAs of the two phage classes differ in structure. In addition, we present our method of calibration of the linear dichroism attachment in the Jasco J-500A spectropolarimeter.

This research was supported by NIH grant GM 19060 and by Grant AT-503 from the Robert A. Welch Foundation.

**M-Pos429**

AN FT-IR MICROSCOPIC DETERMINATION OF THE EFFECT OF FLUORIDE TREATMENT IN OSTEOPOROSIS.
Nancy Pleshko[1], Adele Boskey[2], and Richard Mendelsohn[1]. [1]Department of Chemistry, Rutgers University, Newark College of Arts and Science, Newark, NJ, and [2]Department of Ultrastructural Biochemistry, Cornell University Medical College and The Hospital for Special Surgery, New York, NY.

The use of fluoride in the treatment of osteoporosis (OP) has been a controversial issue. We have applied FT-IR microscopy to study the effects of fluoride on the mineral in OP patients. The phosphate $\nu_3$ mode in the 900-1200cm$^{-1}$ spectral region was used to monitor the hydroxyapatite structure before and after fluoride treatment. Our technique permits characterization of the mineral at up to 20μ spatial resolution.

The predominant mineral in bone is hydroxyapatite (HA), $Ca_{10}(PO_4)_6(OH)_2$. The IR spectra of synthetic HA compounds of different crystallinities were recorded, and their $\nu_3$ absorbances analyzed by curve fitting algorithms. A correlation was found between a subband component of the $\nu_3$ absorbance, and the crystallinity of the HA. As the HA becomes more crystalline, the relative intensity of the feature near 1060cm$^{-1}$ decreases dramatically. This component has been assigned to a disordered phosphate phase.

FT-IR microscopy spectra of the newest mineral in biopsies from OP patients were obtained before and after fluoride treatment. Analysis of the $\nu_3$ mode revealed a large decrease in the relative intensity of the subband resulting from the disordered phosphate phase after fluoride treatment. This indicates a fluoride-induced increase in crystallinity of the bone mineral. FT-IR microscopy is shown to be a powerful diagnostic tool in the evaluation of biomineralization disorders.

**M-Pos430**

## SOLVENT SUPPRESSION IN NMR SPECTRA USING INVERSE FOURIER TRANSFORM EXCITATION

Shenheng Guan and Thomas L. James
*Department of Pharmaceutical Chemistry*
*University of California*
*San Francisco, California 94143*

Rectangular pulses normally used in NMR excitation are nonselective and power consuming. These create technical difficulties for detecting biologically active samples such as domination of solvent peaks in spectra and sample heating. In this work, an inverse Fourier transform method for producing selective and uniform excitation with reduced peak power is presented. The desired excitation frequency magnitude spectrum of the waveform is first specified and the corresponding phase is chosen, so that the peak amplitude is reduced and the power of the waveform is confined within a limited time duration. The waveform is obtained by inverse Fourier transformation of the magnitude and phase spectra. Time evolution of magnetization under excitation and "true" frequency response are examined by solving the Bloch equation. Under the small angle approximation, the true response is proportional to the specified frequency spectra. Our calculations show that the response is almost identical to that specified for a 45° pulse which produces 70% of the signal compared with a 90° pulse. Implementation of the method on a commercial NMR instrument demonstrates the selectivity and flexibility of the method.

**M-Pos431**

## SENSITIVITY IMPROVEMENT IN PROTON DETECTED TWO-DIMENSIONAL HETERONUCLEAR NMR SPECTROSCOPY.

Arthur G. Palmer III, John Cavanagh*, Peter E. Wright and Mark Rance, Department of Molecular Biology, Research Institute of Scripps Clinic, La Jolla, CA and *Department of Chemistry, University of Cambridge, Cambridge, UK.

The sensitivity of proton-detected two-dimensional heteronuclear correlation NMR spectroscopy can be increased by as much as a factor of $\sqrt{2}$, relative to the conventional methods, for heteronuclei with single geminal protons. The enhanced sensitivity is obtained by refocussing and detecting two orthogonal in-phase proton magnetization components, rather than the single component recorded conventionally. The two magnetization components are deconvoluted to produce two pure phase spectra that are added together to produce a spectrum with an enhanced signal-to-noise ratio. Methods of improving the sensitivity of the main classes of single bond heteronuclear correlation experiments are presented and the effect of relaxation during the new experiments on the sensitivity enhancement are discussed. The same methods also can be used to improve the sensitivity of heteronuclear relay experiments that use isotropic mixing to achieve coherence transfer. The new methods are demonstrated by comparing conventional and sensitivity enhanced single bond $^{1}H$-$^{15}N$ heteronuclear correlation spectra of bovine pancreatic trypsin inhibitor at $^{15}N$ natural abundance and by comparing conventional and sensitivity enhanced $^{1}H$-$^{15}N$ heteronuclear relay spectra of uniformly $^{15}N$ labelled enzyme $III^{Glc}$-like domain.

**M-Pos432**

## ASSIGNMENT OF $^{15}N$, $^{13}C$, AND $^{1}H$ BACKBONE AND $^{1}H$ SIDE CHAIN RESONANCES OF $III^{Glc}$ USING HETERONUCLEAR THREE-DIMENSIONAL NMR

Jeffrey G. Pelton§, Dennis A. Torchia§, Norman D. Meadow*, and Saul Roseman*
Bone Research Branch, National Institute of Dental Research, National Institutes of Health §, Bethesda, MD., and The Johns Hopkins University, McCollum-Pratt Institute, Department of Biology*, Baltimore, MD.

$III^{Glc}$, a histidine containing phosphocarrier protein of 168 amino acids participates in the uptake and phosphorylation of glucose in the phosphoenolpyruvate:glucose phosphotransferase system of entric bacteria by shuttling a phosphate group from HPr to a ternary Enzyme II - $III^{Glc}$ - glucose complex. Since there is little information regarding the structure of $III^{Glc}$, we have undertaken assignment of the backbone ($^{15}N$, $^{13}C$, $^{1}H$) and side-chain ($^{1}H$) resonances of this protein and have elucidated several secondary structural elements as a first step in determining it's 3D structure and its mechanism of action.

Complete (98%) backbone assignments were made using the 3D $^{15}N$-HOHAHA-HMQC and a battery of newly developed 3D triple-resonance ($^{15}N$, $^{13}C$, 1H) experiments[1] including the HNCA, HNCO, HCA(CO)N, and the HCACO. The assignments were then extended from the backbone alpha carbon and proton to the side chains using 3D HCCH-COSY[2] and HCCH-TOCSY[3] spectra. Because the triple-resonance and HCCH experiments correlate resonances using only through-bond couplings, the assignments were made without reference to secondary structure. Moreover, only three samples, one fully $^{15}N$ enriched, one fully $^{15}N/^{13}C$ enriched, and one specifically labeled at a few positions with $^{15}N$ and $^{13}C$ were required.

These results show that it is possible to efficiently assign a protein of 18.1kD without the aid of a crystal structure using a combination of heteronuclear labeling and three-dimensional NMR. We are currently analyzing 3D $^{15}N$- and $^{13}C$-NOESY-HMQC experiments to determine the secondary and tertiary structure of this protein.

1 Ikura, M., Kay, L. E. and Bax, A. (1990) *Biochemistry* **29**, 4659.
2 Kay, L. E., Ikura, M. and Bax, A. (1990) *J. Am. Chem. Soc.* **12**, 888.
3 Bax, A., Clore, G. M. and Gronenborn, A. M. (1990) *J. Magn. Reson.* **88**, 425.

**M-Pos433**

## 3D-Localized $^{31}P$ NMR Spectroscopy of Brain and Muscle Using the SLIM Technique - Simultaneous Acquisition of Multiple Regions of Interest.

C. Gregory[1], E. S. Fletcher[2], H. Lee[3], M. J. Dawson[4], D. Levin[5], W. T. Greenough[6] and P. C. Lauterbur[7], Neuroscience Prog.[2,4,6,7] and Depts. of Chem.[3,7], Physiol. & Biophys.[4,6,7], Psychol.[6] and Med. Info. Sci.[1,3,7], U. of I. at Urbana-Champaign and Dept. of Radiology[5], U. of Chicago Medical School.

Spectral Localization by IMaging (SLIM) is a post-acquisition technique which uses information contained in proton images to allow rapid and versatile calculation of physiologically defined spectra within multiple three dimensional volumes. $^{31}P$ SLIM has been previously verified in simple and complex phantoms (Lee and Lauterbur, Biophys. J. 55:452a, 1989) and its robustness has been verified both in computer simulations and complex phantoms (Liang et al., p1077 and Fletcher et al., p1332, Abstracts, 9th Annual Meeting, Society of Mag. Res. in Medicine, 1990). We report here simultaneous acquisition of localized $^{31}P$ spectra in brain and muscle from animal and human subjects.

We are presently using the SLIM technique to obtain spectra of irregularly-shaped volumes of interest of less than 200 µl in a study of brain development in rats. Spectra and images are obtained from anesthetized rats ranging in age from 2 days to adult using a 4.7T, 33 cm bore SISCO imaging spectrometer. Outlining the muscle regions of the head and neck as one volume of interest and brain as another allows calculation of brain and muscle spectra from a small $^{31}P$, phase-encoded, 4-D data set. The phosphorus peak intensities and positions agree with previous NMR and chemical analyses of these tissues. The developing rat brain shows a decrease in phospho-monoesters and increase in phosphocreatine with age, consistent with previous reports.

The human studies are conducted on a Siemens 1.5 T Magnetom using a 17 cm Helmholtz coil for the $^{31}P$ data acquisitions and an orthogonal 20 cm Helmholtz coil for $^{1}H$ imaging. Regional distributions of phosphorus metabolites will be reported.

**M-Pos434**

## RELATIONSHIP BETWEEN FREE INTRACELLULAR MAGNESIUM AND TOTAL MAGNESIUM CONCENTRATION IN SHEEP RED BLOOD CELLS

Phillip Cruz*, Nicholas V. Reo*, Hiroshi Fujise×†, and Peter K. Lauf×
*Department of Biochemistry and Kettering-Scott Magnetic Resonance Laboratory, Wright State University and Kettering Medical Center,
×Department of Physiology and Biophysics, Wright State University
Dayton, Ohio 45435

Intracellular magnesium concentration was investigated in high potassium sheep erythrocytes permeabilized with the ionophore A23187. The cellular free magnesium concentration was measured by $^{31}P$ nuclear magnetic resonance (NMR) spectroscopy, and the total cellular magnesium concentration was determined by atomic absorption spectroscopy. In the concentration range of 0.3 to 1.92 mmol Mg/liter cells, the free and total magnesium concentrations can be expressed as a linear function on a log-log scale. This relationship has the correlation equation: $\log[Mg^{+2}]^F = 2.11 \cdot \log[Mg^{+2}]^T + 1.91$ ($r = 0.984$), where $[Mg^{+2}]^F$ and $[Mg^{+2}]^T$ are the free and total magnesium concentrations, respectively. The method permits the estimation of physiologically or experimentally induced variations of intracellular free magnesium concentrations between 7 and 405 μM magnesium in cell water. This range encompasses the free magnesium concentration of 335±60μM in cell water determined for untreated sheep erythrocytes. The linear relationship does not depend on the value chosen for the dissociation constant of the Mg·ATP complex.

†Current Address: Department of Pathology, School of Veterinary Medicine, Azabu University, Fuchinobe, Sagamihara, Kanagawa 229, Japan

**M-Pos435**

TIME-RESOLVED SPIN PROBE OXIMETRY. Jinjie Jiang, Charles P. Scholes, Janet F. Bank, and Jessica W. Wolpaw, Departments of Chemistry & Physics, State University of New York at Albany, Albany, NY 12222.

An ambient temperature EPR technique is being developed to detect rapid kinetics of $O_2$ consumption. The EPR spectra of small nitroxide spin probes are sensitive to relaxation by dissolved $O_2$[Froncisz et al. (1985) PNAS 82, 411]. We use such spin probes in combination with an EPR stopped-flow system [Hubbell et al. (1987) Rev. Sci. Inst. 58, 1879] based on an Update Instruments ram driver coupled to a sensitive loop gap resonator with microliter sample volume. The enzyme is cytochrome c oxidase, which uses ferrocytochrome c as a reductant and $O_2$ as oxidant to create water. We have used this system for limited turnover experiments where the amount of $O_2$ consumed is comparable to the amount of enzyme (5 micromolar) and where the consumption occurs within less than a second. Experiments in the presence of limiting amounts of ferrocytochrome c show dependence of the initial rate of oxygen consumption upon pH and ionic strength. In the presence of excess ferrocytochrome c and 5 micromolar oxidase about 15 micromolar concentration of $O_2$ was consumed in less than 1 s. The rate of oxygen consumption was constant until the oxygen concentration fell below 1 micromolar. (This work supported by the American Heart Association.)

**M-VCR3**

***in vivo* NMR imaging of magnetically labelled brain cells.**
Ghosh, P.[1,2], Lee, H.[1], Hawrylak, N.[2,3], Greenough, W. T.[2,3], and Lauterbur, P. C.[1,2,3], Biomedical Magnetic Resonance Laboratory[1], College of Medicine[1], Neuroscience Program[3], Beckman Institute[2], University of Illinois, Urbana, IL 61801.

Magnetic iron oxide particles, when introduced into cells, can be monitored by NMR imaging. Such particles induce in their vicinity distortions of the local magnetic field as well as reductions in relaxation times. We have used *in vivo* NMR imaging to observe the fate of iron oxide-labelled fetal neural tissue grafts in the rat brain after intracerebral transplantation, with the goals of monitoring the survival, differentiation and possible migration of transplanted cells.

Donor fetal rat brain tissue were labelled either as intact fragments or as dissociated cells by incubation with reconstituted viral envelopes containing iron oxide particles (mean diameter ~10nm). The labelled tissue fragment or the cell suspension (1-4μl) was drawn up into a glass micropipette attached to a Hamilton syringe and stereotactically injected into the cerebral cortex and/or the dorsal hippocampus of the host rat under Nembutal anesthesia. *in vivo* NMR imaging was performed under Ketamine anesthesia (100-150mg/kg) on the rats in a SISCO 4.7T/33cm bore small animal spectroscopic imaging system, and required 4-5 hours of anesthesia, from which the animals were allowed to recover. 3D FT NMR spin echo (-90°-TE/2-180°-TE/2-echo-TR-; TE=echo time, TR=interpulse delay) and gradient echo (-α-TE-echo-TR-, α=5° to 90° ) images, and 2D FT NMR spin echo (-90-TE/2-180-TE/2-echo-TR-) images (excitation slice thickness ~700μm; TE=30-50ms; TR=4-5s) of the brain of the live adult rats and of the intact fixed brains were obtained using a 3cm(i.d.) surface coil as the receiver and 8.8cm(i.d.) saddle coil as the transmitter. Histological verification of transplants was carried out on brains of hosts that had been aldehyde fixed using Nembutal anesthesia (150mg/kg) and transcardial perfusion. Prussian blue tests for ferric iron were performed on 30μm thick adjacent sections.

The present results demonstrate that populations of iron oxide-labelled cells can be visualized in the NMR images. Images acquired both *in vivo* and after fixation showed dark regions in or around the transplant site. Dark regions were also detected 200-500μm away from the transplant tract along the corpus callosum in the host white matter. Light microscopy confirmed the presence of densely labelled iron-positive cells in regions corresponding to the NMR images. Under high magnification the iron oxide deposits were visible in the soma and new proximal processes of some cells. Within the transplant itself the labelled cells are a heterogeneous mixture of donor neurons and glia, sometimes exhibiting indications of integration into the host tissue. Control studies with unlabelled cell transplants and stab wounds also exhibit similar migratory patterns of iron positive cells along the corpus callosum presumably carrying the iron degradation products of probable hemorrhagic origin released from iron containing proteins. Therefore, the iron-positive cells observed far from the transplant site may be migratory host macrophages.

Acknowledgements: The authors thank Clinton S. Potter of NCSA at the University of Illinois, Urbana, for his help with image processing and 3D visualization, the NCSA for the use of its facilities, and Advanced Magnetics Inc. for the iron oxide preparation.

**M-Pos436**

$^{31}P$ NMR STUDIES OF ISOLATED HEART CELLS: MYOGLOBIN INACTIVATION Beatrice A. Wittenberg and Raj K. Gupta, Albert Einstein College of Medicine, Bronx, NY 10461

We report $^{31}P$ NMR studies of isolated adult rat heart cells carried out on Varian XL-200 and VXR-500 NMR spectrometers. Intracellular high energy phosphates remained stable up to 6-8 hrs. when the cells were loaded in 200 μm diameter polyamide hollow fibers and perfused with nutrient medium. With glucose and pyruvate in the perfusate, gassed with 95% $O_2$ + 5% $CO_2$, isolated heart cells maintained P-creatine/ATP ratio of 1.4 ± 0.1, intracellular pH of 7.13 ± .04 and intracellular free $Mg^{2+}$ of 0.51 ± .04 mM. In glucose containing medium, hypoxia induced by gassing with 100% $N_2$ was accompanied by a reversible decrease in intracellular concentration of ATP (50%) and P-creatine (80%) while the intracellular free $Mg^{2+}$ was reversibly increased by 40%. Thus glycolytic capacity is sufficient to maintain viability in resting heart cells. The addition of iodoacetate (50 μM) in aerobic medium did not significantly alter P-creatine and ATP concentrations. Thus oxidative phosphorylation without glycolysis can maintain high energy phosphate concentrations. 1-2 mM sodium nitrite specifically inactivates intracellular myoglobin but not mitochondrial respiration in heart cells. However, in the absence of functional myoglobin, steady state respiratory oxygen uptake is decreased by about 30%. Here we show that inactivation of intracellular myoglobin caused a significant (30%) decrease in the intracellular P-creatine peak, which was reversed upon removal of sodium nitrite from the well oxygenated perfusion medium. The decrease in P-creatine concentration was also observed in iodoacetate treated cells in the presence of $NaNO_2$, but not in oligomycin-treated myocytes. Since $NO_2$ has no direct effect on creatine kinase, these data suggest that if ATP utilization is unaffected, aerobic high energy phosphate synthesis is diminished in well oxygenated resting heart cells in the absence of functional myoglobin. Supported in part by National Institutes of Health Grant HL-40998.

**M-Pos437**

DIFFRACTION INTENSITY PROFILES FOR MULTI-STRAND HELICES AS A FUNCTION OF STAGGER BETWEEN STRANDS WITH APPLICATION TO MYOSIN. G.F. Elliott, Open University, Oxford Research Unit, Oxford, UK; B.M. Millman, University of Guelph, Guelph, Canada; C.R. Worthington, Carnegie Mellon University, Pittsburgh, PA.

In a new approach to helical diffraction [Acta Cryst. A45:645(1989)] the autocorrelation function (a.c.f.) for a simple helix with point scattering centers was derived. The Fourier transform of the a.c.f. gives the diffraction intensity. This theory has now been extended to multi-strand helices. The theory is simplest when the n-strands have n-fold symmetry (as commonly assumed for the myosin filament). The myosin filament of vertebrate striated muscle however shows extra reflections that are forbidden if the individual strands actually had strict n-fold symmetry. This symmetry can be disordered by introducing a displacement of stagger between individual strands and it is possible that this disordering may give rise to the extra reflections in the myosin pattern. This work is in progress: either, the intensity profiles for myosin obtained by computer will be shown, or else, the basic theory of the method of calculation will be described.

**M-Pos438**

X-RAY AREA DETECTOR DEVELOPMENT
Walter Phillips, Martin Stanton, Youli Li, and Kenneth Kalata, Rosenstiel Basic Medical Sciences Research Center, Brandeis University, Waltham, MA 02254

We have designed and built two x-ray area detector systems which are currently operating in our laboratory: an intensified CCD-based system designed for either synchrotron or laboratory sources, and an intensified SIT vidicon-based system designed for laboratory sources. The CCD-based detector has a 75 mm diameter area which is imaged onto a Videk 1035 X 1320-pixel CCD camera using two image intensifiers, a fiber optic reducer and a lens. The resolution is ~800 X 800 pixels and the output is digitized to 12 bits. The vidicon detector camera has an 80 mm diameter active area, and can be operated in either a conventional TV (analog-to-digital) mode utilizing a 12 bit A/D converter with a resolution of ~150 X 180 pixels, or a photon-counting mode with resolution of ~800 X 800 pixels. Using MADNES, Rsyms are typically 3 - 4% for 90-degree data sets to 3 A resolution on tetragonal lysozyme or cubic insulin, with all observed reflections included. A more useful measurement of detector performance is provided by the Detective Quantum Efficiency (DQE), which ranges from 0.8 at high gain and high counting rates to 0.1 at low gain and low counting rates.

An advanced CCD-based detector optimized for use with laboratory sources is being constructed. The camera will have a 115 mm diameter and use a Tektronics 1024 X 1024-pixel CCD. All optical elements will be directly coupled with fiber optics, increasing the light transfer efficiency between x-ray converter and CCD. The CCD will be readout at 500 KHz and digitized to 12 bits. All of the deetctor systems are designed to utilize the same software for detector control, data collection and data processing.

M-Pos439

# WIZARD

## Artificial Intelligence and Axiomatic Logic in Conformational Analysis

D. P. Dolata, Ajay Shah

WIZARD is a conformational analysis program based on principles of Artificial Intelligence and Axiomatic Logic. Given a molecule, it examines its axiomatic data base to find those basic principles of conformational analysis which are appropriate for this molecule. It then logically combines these axioms following a hierarchical plan, performing self criticism of the partial results as it proceeds. If WIZARD succeeds in criticizing an intermediate result, this constitutes a proof that the axioms were incorrect or insufficient. If WIZARD decides that the fault lay in an insufficiency of knowledge, it then attempts to augment it's axiomatic data base by learning a new axiom from the example. The end result of any WIZARD session is a set of all stable conformations for the given molecule, and possibly an augmented set of axioms of conformational analysis. The logically based predictions typically agree with experimental data (e.g. X-Ray) to within 0.25Å RMS. The results may be further refined by accepted mathematical methods (MM2, MOPAC) to obtain better energetic values. The combination of WIZARD and a mathematically based program has been shown to be very efficient.

The utility of WIZARD is being demonstrated by addressing a number of biophysical problems such as:

**Atherosclerosis** - lipid conformations and the ability of various lipids to form stacking groups. The conformations of cholesteryl compounds.

**Pharmaceuticals** - solution conformations of medium sized alkaloids and terpenoids.

**Multi Drug Resistance in Chemotherapy** - utilization of WIZARD's ability to generate ALL conformations of a compound, coupled with a new logico-deductive approach to map out the shape of the PGP receptor(s) responsible for MDR in tumors.

M-Pos440

COMPUTER MODELING OF TRANSLOCATING INTRACELLULAR FLUORESCENT PROBES IN ROUND CELLS. James L. Weaver, CDER, Food & Drug Administration, Washington, DC.

The intracellular distribution of certain molecules such as protein kinase C has definite biological importance. Fluorescent probes can be used to mark the location of such molecules, however quantitation of the resulting information can be difficult. Fluorescence line scan profiles of cells can be used to obtain information about the intracellular location of the fluorescent probe. These profiles can be obtained experimentally using laser scanning fluorescence microscopes.

Model fluorescence line scan profiles for probes with various defined percentages of distribution between the cytoplasm and the cell membrane or between cytoplasm and the nuclear membrane have been calculated for round cells. These calculations show large differences in the profiles expected between all cytoplasmic and all membrane distributions of fluors. These differences have been quantitated by calculating the slope of a linear regression line for data in a specific region of the profile. The results show that there is a linear relationship between these slopes and the percentage of fluor in the cytoplasm and associated with the membrane.

Actual cell profiles from round cells obtained using fluorescent probes with known cell membrane (NBD-phosphatidyl choline or PE-labeled monoclonal antibodies) or cytoplasmic (Fluo-3 or NBD-glucosamine) distribution show good agreement with the calculated data. In conjunction with the profiles of cells labeled with molecules of known distributions, these measures can be used to quantitate the proportions of fluor found in the cytoplasm and associated with the cell or nuclear membrane. This method is applicable to any situation where knowledge of the intracellular distribution of a fluorescently-labeled probe would be useful.

M-Pos441

E. COLI PROMOTER PREDICTION USING A NEURAL NETWORK.

Borries Demeler and Guangwen Zhou
(Intro. by Dr. Ken van Holde)
Department of Biochemistry and Biophysics
Oregon State University
Corvallis, OR 97331

An artificial neural network is presented to predict *Escherichia coli* RNA polymerase promoter sequences. The neural network was trained on a set of 81 known promoter sequences and a variable number of random sequences. The conserved -10 and -35 regions of the promoter sequences and a combination of these regions were used in three independent training sets. The prediction accuracy of the resulting weight matrix was tested against a separate set of 30 known promoter sequences and 1500 random sequences. The neural network formulation was optimized for this task with respect to following parameters:
1.) network architecture
2.) extent of training
3.) ratio of random sequences/promoter sequences
4.) data representation
Accuracies of 100% on the promoter test set and 98.4% on the random test set were achieved in the optimal environment. A consensus sequence obtained from analysis of the learned weight matrix is presented.

M-Pos442

COMPUTER MODEL OF BASILAR ARTERY ANEURYSM:
EFFECT OF SIZE ON INTRA-ANEURYSM FLOW

George Austin & Robert Gaskell, Stroke-Aneurysm Research Foundation (UCSB) and Dept. of Neurosurgery (UCSB)

An elliptic human basilar aneurysm was developed from angiographic data and our modification of Raines (1974) use of the non-linear Navier-Stokes and continuity equations for measuring arterial pressure and flow in the human leg. Aneurysms varied from 4-32 mm. in length. Pressure and flow pulse waves were measured at 2 mm. intervals in the parent arteries and within the aneurysm.

The input function was a pressure pulse wave (PPW) with B.P. of 120/70 and pulse rate of 92/m. Wall compliance and inertance were maximum at the equator in the 8 aneurysms studied. Computer solution of the model showed peak flows of 9.5 - 11.0 cc/s at the basilar artery (BA) tip, and 4.3 - 4.5 cc/s in the proximal past-cerebral arteries (PPCA). Intra-aneurysm (IA) mean flow varied from 0.3 cc/s in the shortest (4 mm.) up to 1.9 cc/s in the longest (30 mm.). IA flow was maximum at the neck and decreased to 46% at the dome. IA pressure did not change significantly. IA flows of 3-17% of basilar tip flow are against high velocity turbulent flow. Any IA chemically secreted factor would be washed out more rapidly at the neck and minimally at the dome since flow near the dome is decreased by 54%.

M-Pos443

**DIFFUSE PHOTON TRANSPORT IN TURBID MEDIA: EXPERIMENTS AND MODEL VERIFICATION.** J. Fishkin, M. vandeVen and E. Gratton. *Laboratory for Fluorescence Dynamics, Department of Physics, University of Illinois at Urbana-Champaign, 1110 W. Green Street Urbana, IL 61801.*

It has recently been shown that the multi-frequency cross-correlation spectroscopy technique can succesfully be used to obtain images in the near-infrared region of tissues and phantoms. So far the properties of the photon diffusion process are not completely understood although the transport equation can be applied to a certain extent and the general shape of the various relationships is reproduced correctly. The solution of the diffusion approximation to the linear transport equation with an intensity-modulated point source indicates that intensity-modulated light in turbid media can be treated within the framework of wave phenomena. To further elucidate the observed physical phenomena and to test the validity of the underlying theory, we have carried out near-infrared transmission experiments on highly scattering skim milk emulsions and absorbing emulsions containing varying quantities of india black ink. Phase shifts, demodulation and intensity data were collected for a range of frequencies from 20 MHz to 400 MHz at regular intervals. The illuminating light source was a synchronously-pumped, cavity-dumped rhodamine 6G or LDS 698 (pyridine 1) single-jet dye-laser running at a pulse repetition rate of about 2 MHz. (Supported by NIH grant RR03155).

M-Pos444

**NEAR-INFRARED IMAGING SPECTROSCOPY OF MAMMALIAN TISSUE IN THE FREQUENCY DOMAIN.** M. vandeVen, T. French, J. Fishkin and E. Gratton. *Laboratory for Fluorescence Dynamics, Department of Physics, University of Illinois at Urbana-Champaign, 1110 W. Green Street, Urbana, IL 61801.*

It has recently been shown that modulated near-infrared (NIR) light generated by a multi-frequency cross-correlation spectrometer can successfully be used to obtain two-dimensional projections of the internal structure of turbid, highly scattering media such as thick mammalian tissues. To further explore the physical phenomena related to the transport of diffuse radiation in such tissues we have carried out NIR transmission experiments. The illuminating light source was a synchronously-pumped, cavity-dumped Rhodamine 6G or LDS 698 (pyridine 1) single-jet dye-laser running at a pulse repetition rate of about 76 MHz. Total power impinging on the test objects was less than 100 $mW/cm^2$. Surfaces of objects were scanned with home-built x-y scanning devices and with array-detectors, both interfaced with fiberoptics. The large data sets, typical size on the order of Mbytes, were processed with commercially available and home-written fast image analysis software. Images of a whole hand are presented as obtained from the transmitted intensity, phase shift and demodulation for various modulation frequencies and pre-selected illumination colors. Each measured parameter unveils different details of the various internal structures, e.g., muscle, bone and arteries. Present limitations and limits of resolution of this non-destructive, non-invasive NIR imaging technique with potential direct applications of real-time imaging of tissues of medical importance are discussed. (Supported by NIH grant RR03155).

M-Pos445

A LASER HETERODYNING DETECTOR FOR FREQUENCY-DOMAIN FEMTOSECOND SPECTROSCOPY. K. Berland, M. Dowling,* M. vandeVen and E. Gratton. Laboratory for Fluorescence Dynamics, University of Illinois at Urbana-Champaign, 1110 W. Green Street, Urbana, IL, 61801 and *Department of Nuclear Engineering and Health Physics, ESM-G-4, Georgia Institute of Technology, Atlanta, GA 30332.

Ordinary heterodyning and superheterodyning methods in the frequency domain are limited mainly by the response of the detector. The replacement of the photomultiplier detector by 6 micron microchannelplate photomultiplier detectors has improved the frequency response from 500 MHz to 10 GHz. We have developed a new method in frequency-domain spectroscopy to detect the fastest absorption processes by extending to the frequency-domain the well-known pulse-probe technique used in the time-domain which is based on the use of a variable delay line. Two mode-locked Coherent Neodymium-Yttrium Aluminum Garnet (Nd-YAG) lasers, operating at a slightly different mode-lock repetition frequency, together with an inexpensive Hamamatsu side-on photomultiplier are used to detect changes in absorption caused by a strong bleaching laser pulse and probed by another phase-locked laser of far lesser intensity. The upper frequency limit attainable is only limited by the pulse width of the light sources. For picosecond excitation sources it extends to hundreds of GigaHertz. Examples are shown for samples with fluorescence lifetimes ranging from nano- and picoseconds such as rhodamine 6G, rose bengal, pinacyanol, to femtoseconds (porphyrins). The derivation of the basic equations for the laser heterodyning detector are given in the frequency domain. This work is supported by NIH grant RR 03155.

M-Pos446

**OXYGEN IMAGING IN TISSUE.** Jenny Carrero and E. Gratton. *Laboratory for Fluorescence Dynamics, Department of Physics, University of Illinois at Urbana-Champaign, 1110 W. Green Street, Urbana, IL 61801.*

The dependence of higher animals on oxygen arises from cellular metabolism. The circulatory system and oxygen-carrying molecules deliver oxygen to the cells. A better understanding of the mechanisms that regulate oxygen delivery to the tissue will be achieved with more accurate measurements of intercellular and intracellular oxygen concentrations. The possibility of imaging oxygen in tissue is being explored using frequency domain phosphorimetry. The phosphorescent probe Palladium Coproporphyrin (PDCO) has been used for its triplet state lifetime dependence on oxygen concentration (Vanderkooi, 1987). We have performed experiments using tissue from rat livers that were perfused with a solution containing PDCO. A configuration of optic fibers was arranged such that a two-dimensional raster scan of the average pixel phosphorescence was obtained from the tissue. An image of the phosphorescent intensity from the liver slice has been obtained using the DC measurements for each. Phase and Modulation experiments will be performed using the same configuration to get spatial resolution of lifetimes within the tissue. This resolution is limited to the size of the pixel. The lifetime map can be correlated to the average concentration of oxygen in the tissue. (Supported by NIH grant RR 03155 and PHS 5GM10715-02).

**M-Pos447**

THE RAMAN SPECTROSCOPY OF INDIVIDUAL AMINO ACID RESIDUES IN POTEINS. J. A. Ball, D. J. Weber, A. S. Mildvan, R. H. Callender. Physics Department (J.A.B. & R.H.C.), City College of the City University of New York, New York, NY 10031. Department of Biological Chemistry (D.J.W. & A.S.M.), Johns Hopkins Medical School, Baltimore, MD 21205

We are exploring the feasibility of obtaining the Raman spectra due to a specific amino acid residue within proteins. By subtracting the Raman spectrum of a site specific mutant from that of the native protein, a difference spectrum is generated in which positive bands are the result of the target residue in the native protein and the negative bands are due to the mutated residue. Since we employ classical Raman scattering, the selection of probed residues is quite general and is not limited by a specific resonance absorption. At present we have obtained the Raman difference spectra between a wild-type and a glutamate-43 to serine mutant of staphylococcal nuclease. These difference spectra show vibrational bands attributed to the carboxalate of glutamate's side group which is expected to be sensitive to the local hydrogen bonding: The carboxalate is proposed to act as a general base in the catalytic mechanism by properly coordinating of the water ligands to the metal cation at the active site. Using Raman difference spectroscopy of free, unbound versus enzyme bound substrate, we have previously shown shifts in a substrate's vibrational frequency upon binding; currently, we are also investigating the effect of mutation on the vibrational bands of the bound inhibitor, thymidine 3',5'-diphosphate, in the ternary nuclease-($Ca^{2+}$)-inhibitor complex. Because of the similarity between wild-type and mutant enzyme spectra, a discussion of the present experimental technique in relation to the observed and expected signal sizes in these difference spectra will be included.

**M-Pos448**

ENHANCEMENT OF FLUORESCENCE RECOVERY AFTER PHOTOBLEACHING TECHNIQUES FOR MEASURING FAST DYNAMICS.

Ariane Mc Kiernan, Yifeng Yuan, and Daniel Axelrod, Biophysics Research Division and Dept. of Physics, University of Michigan, Ann Arbor, MI 48109.

Optical and electronic modifications of two variants of fluorescence recovery after photobleaching (FRAP) microscopy techniques have been made to allow measurement of more rapid kinetic processes than previously possible.

The first is a modification of TIR (total internal reflection)/FRAP, which measures desorption and surface diffusion kinetics of molecules reversibly adsorbed at a solid/liquid interface. "Prismless" TIR by epi-illumination through a high aperture objective (introduced previously by Stout and Axelrod, 1989, *App. Opt.* 28: 5237) here utilizes two intersecting laser beams which form interference fringes in the evanescent field of TIR. The fringes are considerably smaller (0.3 $\mu$m spacing) and more stable than previously attainable, thereby allowing surface diffusion rate measurements on samples with faster adsorption/desorption kinetics.

The second modification is an extension of polarized FRAP for measuring rotational diffusion down to tens of nanosecond time scales. We find that a very brief (0.5 ns) visible laser light pulse of high intensity (~10 $\mu$J/pulse) can easily bleach rhodamine-labeled protein. Because the bleaching pulse is shorter than the fluorescence lifetime, this suggests that a two-photon excitation to a very bleachable state may be involved. A versatile hardware and software system utilizing automated computer and trackball control of stage position, separation of the polarized bleaching and probe light paths, concurrent pulsed nitrogen/dye laser and CW argon laser sources, and digital storage oscilloscope data aquisition, allows efficient gathering of rotational diffusion data on biological samples on time scales ranging from tens of nanoseconds to many seconds. Supported by NIH NS 14565 and NSF DMB 8805296.

**M-Pos449**

A RAPID-FLOW X-RAY ABSORPTION SPECTROSCOPY TECHNIQUE WITH MICROSECOND RESOLUTION

Daniel J. Thiel,[1] Peter Livins,[2] Aaron Lewis,[1,3] and Edward A. Stern.[2] [1]School of Applied and Engineering Physics, Cornell University, Ithaca, NY 14853; [2]Dept. of Physics, University of Washington, Seattle, WA 98195; [3]Dept. of Applied Physics, Hebrew University, Jerusalem Israel.

A new technique is presented for obtaining time-resolved x–ray absorption fine structure (XAFS) data on photo-activated molecules. XAFS is a technique that can give extremely precise structural information in the neighborhood of selected atoms without the need for crystallization. By obtaining time-resolved XAFS spectra, one could determine structural changes in molecules with detail not obtainable with any other method as well as the corresponding kinetics. Our new method can be applied to proteins and enzymes which contain metal atoms to determine the structural changes that take place near the metal atoms on a one microsecond time scale.

The method involves flowing a solution containing the molecule of interest through a nozzle to form a free-standing jet and shining a focused laser beam onto the jet to excite the molecule. The excited state is probed by directing an x–ray beam at the excited region. By vertically displacing the pump beam relative to the x-ray beam, one controls the time delay between the excitation and the probe. The time resolution is determined by the flow velocity and the size of the x-ray beam. In our initial studies, a flow velocity of 20 m/sec and an x-ray beam size of 10 μm were used to study the long-lived (10 μsec) triplet state of the inorganic species, $Pt_2(P_2O_2H_2)_4^{4-}$.

**M-Pos450**

**POSITRON ANNIHILATION LIFETIME STUDIES OF PROTEIN HYDRATION.** **Roger B. Gregory and Wen Su, Dept. of Chemistry, Kent State University, Kent, Ohio 44242.**

When positrons enter condensed matter they rapidly lose their kinetic energy by collision until they reach thermal energies, at which point, some fraction form singlet or triplet $e^+e^-$ bound states (positronium). The triplet state, or o-Ps, has a free-space lifetime of 140 ns, but this is reduced to 0.5 to 10 ns in condensed matter as a result of "pick-off" annihilation processes, in which an electron of appropriate spin from the medium is capture resulting in rapid subsequent annihilation. o-Ps lifetimes are therefore sensitive to electron density and reflect the probability of Ps-electron encounters. o-Ps traps in packing defects and regions of free volume and its lifetime is a measure of the size of the free volume regions. We have determined positron annihilation lifetime distributions for lysozyme as a function of hydration. o-Ps lifetimes in dry lysozyme are broadly distributed suggesting a distribution of free volume sizes up to 170 $A^3$ (i.e radii up to 3.5 A). The average lifetime equals 1.74 ns which corresponds to an average free volume size of 63 $A^3$. In the fully hydrated protein the distribution of o-Ps lifetimes is narrower and the average lifetime is shifted to 2.15 ns (120 $A^3$). The dry protein is conformationally rigid. The distribution of free volume is therefore "frozen". Water acts as a plasticizer of the protein and beyond a critical hydration level, fast (sub-ns) conformational rearrangements lead to free volume averaging and a decrease in the o-Ps peak width. The increase in average o-Ps lifetime on hydration may reflect the free volume of the hydration layer (unlikely, because o-Ps lifetimes in water and ice are considerably less than 2.0 ns), a change in the distribution of intrinsic, unperturbed free volume of the protein or an expansion of protein free volume regions due to repulsions between o-Ps and the flexible surrounding protein (Ps bubble formation).
(Supported by NSF grant DMB 85-18941 and ARO grant DAAL03-90-G-0061)

M-Pos451

NOVEL STABLE ISOTOPE METHODS FOR QUANTITATING CELLULAR FATTY ACID AND CHOLESTEROL SYNTHESIS.
J.K. Kelleher, T.M. Masterson, and A.T. Kharroubi., George Washington U. Medical Center, Washington, D.C.

Incorporation of 14C carbon tracers (e.g., acetate) into fatty acids and cholesterol does not yield true estimates of the rate of synthesis because the specific activity of the intracellular precursor pool (acetyl CoA) is unknown. In contrast, experiments utilizing 13C precursors and specific ion monitoring gas chromatography/ mass spectrometry provide the contribution of the tracer to the endogenous precursor pool and the rate of synthesis of product (Strong, J.B.C., 260: 4276, 1985). This property is a consequence of the fact that the product contains more than one precursor molecule; 8 acetate --> 1 palmitate, for a typical fatty acid, and 10 acetate + 7 individual acetate carbons --> 1 cholesterol. Equations based on probability functions yield estimates for 2 parameters, (F) fractional contribution of the tracer to the precursor pool and (G) fractional contribution of the newly synthesized material to the product. Graphed below are possible values for F and G from 5 equations for experimental data, masses m+0 to m+4 for palmitate synthesized in media containing [2-13C]pyruvate. Ideally, all lines intersect at a point; in practice, parameter estimates are obtained by minimizing the sum of square error. For this example, F = 0.25, indicates that tracer pyruvate provided 25% of the acetyl CoA used for new palmitate synthesis; G = 0.06 indicating that 6% of the total palmitate was synthesized during the incubation. In addition to pyruvate tracers, equations have been developed for the synthesis of cholesterol from [4,5-13C]mevalonate. These equations have been used to evaluate sources of carbon and rates of lipid synthesis in 3T3-L1 adipocytes and AS-30D tumor cells.

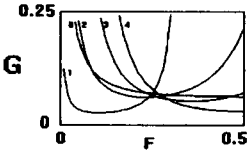


M-Pos452

PC BASED DATA ACQUISITION SYSTEM FOR REAL-TIME INTERFEROMETRY IN THE ANALYTICAL ULTRACENTRIFUGE
Jeffrey Lary, Jia-Wen Wu and David Yphantis, Molecular and Cell Biology and Analytical Ultracentrifuge Facility, University of Connecticut, Storrs CT 06269-3125

A system for automated measurement of Rayleigh interference patterns has been built from readily available, moderately priced commercial components. It requires little fabrication. The interferometric light source is a near infrared laser diode pulsed so as to illuminate the desired ultracentrifuge cell. A CCD camera views enlarged radial sections of the interferometric image. This camera is positioned by a stepping-motor equipped stage. Video images are digitized by a "frame grabber" connected to a 386-type PC which performs Fourier analyses to obtain 512 fringe displacements in less than 6 seconds. The reproducibility of measurements is better than 0.005 fringe with precision better than 0.01 fringe. This PC also provides ancillary services including image calibration, camera setup, correction for angular misalignment and automated timed data acquisition from multiple channels and/or cells. It also communicates via RS-232 lines with an 8088-type PC that, in turn, provides direct control of laser timing and stepping motor action.

Supported by NSF grants DIR-8612159 and DIR-8717034.

M-Pos453

LAMDA (LASER AMPLIFIED MOTION DETECTION AND ANALYSIS) STUDIES OF THE BASILAR MEMBRANE IN THE RED-EARED TURTLE.
Michael P. O'Neill and Alan Bearden. Department of Molecular & Cell Biology (Neurobiology Division) and Graduate Group in Biophysics, University of California, Berkeley, CA 94720.

The first stage of frequency separation in mammalian auditory transduction is the frequency-dependent pattern of movement of the basilar membrane (BM). In nonmammals, this is not necessarily the case. For example, in the turtle, an electrical resonance in the receptor cell membrane partially accounts for the process of frequency sorting (Crawford & Fettiplace, *J. Physiol. (Lond.)* 312:377, 1981). But how much, if any, of this sorting in the turtle is done mechanically by its BM?

To answer this question, we have constructed a prototype device to map the motion of the turtle BM, point-by-point, ultimately leading to a three-dimensional reconstruction of the exhibited waveform. The device is based on the ability of a small amount of optical feedback from an external reflecting surface (target) to modify the output intensity ($I_o$) of a He-Ne laser. For small oscillations of the target, the modulation of $I_o$ is characteristic of the amplitude and frequency of the target's motion. The effect, named LAMDA, is essentially linear for changes in target position of less than ~$\lambda/8$ of the laser light wavelength and has been observed easily for vibrations as small as ~10pm; motions of the turtle BM at the threshold of hearing are ~100pm or less (Crawford & Fettiplace, *Hear. Res.* 12:199, 1983). Because LAMDA requires only a small amount of back-reflected light to reenter the laser ($10^{-6}$% - 1%), we can easily measure the motion of diffuse scattering surfaces; diffuse reflection from the BM provides ~0.01% feedback (Khanna *et al., Acta Oto-Laryngol. Suppl.* 467:69, 1989). LAMDA measurements of BM motion also do not present the problems associated with previous methods such as capacitance probes, the Mössbauer technique, and traditional laser interferometry. In addition, LAMDA's sensitivity will allow us to study at and near threshold sound levels (~0-30dB SPL), unlike most previous methods. This is important in discerning any transition that may exist between linear and nonlinear behavior of the BM.

M-Pos454

## A METHOD FOR MEASURING SUB-NANOMETER FEATURES OR MOTIONS OF BIOLOGICAL STRUCTURES.
M. P. O'Neill[1], L. C. Osborne[1], T. L. Wong[1], and Alan Bearden[2].

[1] Graduate Group in Biophysics, U. C. Berkeley, Berkeley, CA
[2] Division of Neurobiology, Department of Molecular and Cell Biology, U. C. Berkeley, Berkeley, CA.

We present a technique for imaging biological structures to better than nanometer resolution using Laser Amplified Motion Detection and Analysis (LAMDA). LAMDA is an interferometric effect that measures target motion or position along the axis of the beam by means of the back-scattered light's interaction with the laser cavity causing a modulation of the laser output intensity. The laser power response is essentially linear for surface feature changes of less than $\lambda/8$ and is a well-characterized non-linear function of target position and motion as small as picometers and up to many wavelengths. We present a summary of the physics involved in the technique with experimental support both by us and by other groups who have used LAMDA for Doppler velocimetry, mode stabilization in lasers, measuring spherical aberration of lenses, etc.. LAMDA is particularly advantageous for the investigation of biological samples: only 1%-$10^{-6}$% of the beam intensity needs to reflect into the laser cavity, samples need not be fixed or dehydrated as in other microscopy techniques requiring vacuum conditions and in fact samples may be immersed in solution, low power lasers (1 mW HeNe gas lasers or laser diodes for example) are sufficient, avoiding problems of radiative damage to biological structures. Applications to biological motion and structure studies and to microscopy will be discussed.
This research is supported by the N.S.F.

**M-Pos455**

THE CHARACTERIZATION OF ANTIBODY-ANTIGEN INTERACTIONS BY A NOVEL BIOSENSOR TECHNOLOGY: BIACORE™. T. Knower*, J. Carlson*, D.M. Yarmush*, M.L. Yarmush*, and R. Granzow. *Department of Chemical and Biochemical Engineering, Rutgers University and The Center for the Advancement of Biology and Medicine, Piscataway, NJ 08855 and Pharmacia Biosensor NA, Piscataway, NJ 08855-1327. (Intro. by K. Korkidis, Pharmacia Biosensor NA).

Monoclonal antibodies (mAbs) are finding increasing use as primary tools for the identification, assay and purification of a variety of antigens. In all of these applications, mAb characterization (e.g. equilibrium binding constant, association and dissociation rate constants, epitope location) may play a crucial role in determining the operating parameters for a given task. The capability for rapid and accurate mAb characterization has recently been enhanced by the introduction of an instrument which performs real time measurements of antibody-antigen interactions. This new technology called BIAcore is based on advances in three areas: fluidics, biospecific matrices and surface plasmon resonance detection. Micro-fluidics have been optimized for low characteristics and reproducibility to yield accurate interaction analysis in ul volumes. The sensor chip gives a regenerable biospecific matrix that is coupled directly to the detector system. The detection system is based on the optical phenomenon, surface plasmon resonance (SPR). This phenomenon, when coupled to the sensor chip, makes real-time, label-free Biospecific Interaction Analysis (BIA) possible.

Using this instrument we have measured the change in the SPR signal for several mAb-antigen pairs interacting with BSA and have calculated the on-off rates as well as the binding constants of these systems. Preliminary results show that binding constants obtained from kinetic data for some mAbs are similar to those values obtained using radioimmunoassay. Techniques for optimization of concentrations flowrate, pH and data analysis will also be discussed. The benefits of this system, BIAcore, are low sample consumption, no requirements for labelling of interactants and high precision.

**M-Pos456**

Deuterium Exchange on Micrograms of Protein by ATR IR Spectroscopy on Silver Halide Fibers

by Stella M. Chiacchiera and Edward M.Kosower

Biophysical Organic Chemistry Unit
School of Chemistry, Tel-Aviv University
Tel-Aviv 69978 Israel

Two monolayers of trypsin(10μg) on a silver halide optical fiber (0.9mm) yield a good IR spectrum by ATR (attenuated total internal reflectance) using ZnSe lenses and a TGS detector. The exchange of ND for NH induced by flowing $N_2$ gas saturated with $D_2O$ can be followed and reaches the fast limit in ca 30 minutes. A difference spectrum (initial-final) reveals NH loss and ND gain in three spectroscopic regions, NH stretching, C=O stretching (H-bonded) and NH bending. Flowing $N_2$ + $H_2O$ leads to the initial spectrum, with a difference spectrum which is the mirror image of the first.

Exchange of ND for NH in soy bean trypsin inhibitor is slower [for the fast exchange] and proceeds to a lesser extent. The combination of trypsin with the inhibitor produces a complex which exchanges less than either component. Approximately 30-40% of the rapidly exchanging protons are protected from exchange in the complex.

The trypsin is enzymatically active (no buffer) after 24 hours on the fiber and shows no degradation by electrophoresis. Applications of the technique will be discussed.

**M-Pos457**

ON PHOTOCLEAVABLE, HETEROBIFUNCTIONAL CROSSLINKING REAGENTS AND THE PREPARATION OF *CAGED PROTEIN* COMPLEXES.
Gerard Marriott. (Introduced by K. Kinosita). Department of Physics, Keio University, 3-14-1 Hiyoshi, Yokohama 223, Japan.

Cleavable crosslinking reagents are often used to prepare complexes of non-interacting proteins in which the activity of each protein is preserved. If, however, the activity of one or more protein is physically blocked upon complex formation, and if cleavage of the complex relieves this inhibition, then these inactivated crosslinked protein complexes maybe described, somewhat loosely, as *caged protein* complexes. Complexes of this type, which undergo either a chemical or photochemical based cleavage have already been reported (Baldwin *et al, Meth. Enzymol. 133*, 248. 1986 and Senter *et al. Photochem. Photobiol. 42*, 231 1985). Photocleavable *caged protein* complexes may be used to rapidly trigger biological activity in living cells or tissue with sub-micron spatial resolution and diverse applications in cell biology are envisioned. To further investigate these reagents and the reactivation of proteins inhibited in photolabile crosslinked complexes I have synthesised a reagent which incorporates a 2-nitrobenzyl group for photocleavage and NHS-ester and bromoalkane groups for specific couplings to amino and thiol groups. This reagent has been used to crosslink, very efficiently, upto 13 actin monomers in F-actin filaments. Using SDS-PAGE analysis I have shown these *caged* actin oligomers are photochemically converted to functional monomeric actin molecules in F-actin, or as G-actin units in G-buffer.

One general approach to inhibit the activity of a protein is to mask its active site using an avidin complex prepared by specifically labelling the protein of interest with a thiol reactive photocleavable biotin derivative, and then adding avidin. Thus preliminary studies indicate a G-actin conjugate of this biotin derivative is capable of undergoing salt-induced polymerisation to F-actin in the absence, but not in the presence of avidin. This particular candidate will be studied in detail to evaluate the potential of triggering biological activity in cells. Details of the synthetic, spectroscopic and cleavage properties of these reagents and their complexes, along with ongoing research in this area will be presented.

**M-Pos458**

THE ANALYSIS OF PHOTOCHEMICAL PROCESSES
Ogden G. Brandt[1] and Ranieri Rolandi[2].
[1]St. Lawrence University, Canton, New York 13617
[2]Dipartimento di Fisica, Universita di Genova, Genova, Italy 16146.

The analysis of photochemical processes often replaces first order chemical kinetic equations by electrical circuits because the differential equations are identical. The most general case for a set of N first order kinetic equations is discussed, with attention paid to the physical meaning of the time constants, variables and inhomogeneous terms in the differential equations. An alternative approach is to numerically integrate the N kinetic equations: this allows for second order chemical reactions as well as voltage dependent rate constants. A non-linear fitting routine is easily adapted to fit the constants to the data; a side benefit is the ability to follow the time course of each of the chemical species during the process. We show an example of the range of fits possible with this method for CdS deposited on one surface of a BLM, using four coupled chemical reactions.

**M-Pos459**

**A FITTING FUNCTION FOR THE ANALYSIS OF SEDIMENTATION VELOCITY CONCENTRATION DISTRIBUTIONS FROM THE ANALYTICAL ULTRACENTRIFUGE.**
Arun K. Attri and Marc S. Lewis, LC, NHLBI and BEIP, NCRR, National Institutes of Health, Bethesda, MD 20892.

The use of data acquisition systems for recording from the absorption optical system of the analytical ultracentrifuge provides data superior in both number of data points and in precision to that obtainable by manual digitization of the strip chart recording. We find that sedimentation velocity data so obtained is frequently well fit by the function

$$c(r,t) = \sum_{i=1}^{m} c_{p,i,t} \exp(n_{i,t}(r^2 - \bar{r}_{i,t}^2)) / (1 + \exp(n_{i,t}(r^2 - \bar{r}_{i,t}^2))) + c_{b,t}$$

where $c_{p,i,t}$ is the concentration in the plateau region, $c_{b,t}$ is the baseline concentration, $n_{i,t}$ is a parameter related to the diffusion coefficient and $\bar{r}_{i,t}$ is the radial position corresponding to the second moment of the mass in the sedimenting boundary provided that the condition $r_p^2 = 2\bar{r}^2 - r_m^2$ is met. This, as well as the general quality of the fit, is best evaluated by examination of the distribution of the residuals. The value of the sedimentation coefficient is obtained by analysis of $\bar{r}_{i,t}$ as a function of time.

A graph equivalent to a schlieren pattern can be obtained by plotting

$$dc(r,t)/dr = \sum_{i=1}^{m} 2 c_{p,i,t} n_{i,t} r \exp(n_{i,t}(r^2 - \bar{r}_{i,t}^2)) / (1 + \exp(n_{i,t}(r^2 - \bar{r}_{i,t}^2)))^2$$

as a function of radius. This plot combined with plots of the individual terms in the summation is particularly useful for evaluating the data obtained from paucidisperse solutions. The diffusion coefficient is related to $n_{i,t}$ and $\bar{r}_{i,t}$ by $n_{i,t}\bar{r}_{i,t} = 1/(\pi D_i t)^{1/2}$, and the value of the diffusion coefficient is obtainable by appropriate fitting procedures.

**M-Pos460**

NETWORK THERMODYNAMIC MODEL SUPPORTING THE SUPEROXIDE THEORY OF OXYGEN TOXICITY.
Suzuki, Y. and Ford, G. D., Department of Physiology, Medical College of Virginia, Richmond, VA 23298.

McCord and Russell recently reemphasized the superoxide ($O_2^-$) theory of oxygen toxicity stating that: "$O_2^-$ is not a highly reactive free radical. The hydroxyl radical ($HO\cdot$), by contrast, has almost unlimited reactivity, but on a mole-for-mole basis this does not necessarily imply greater toxicity. A cell may recover very well after loosing 5% of every enzyme activity, but it may not recover at all after loosing 95% of one particularly vital enzyme activity. Reactivity and toxicity are, to a large degree, inversely related." The present study presents a mathematical model depicting such a situation. The 'biological response' is presumed to be the result of a linear sequence of 10 unimolecular subreactions, i.e. A -> B -> C -> D -> E -> F -> G -> H -> I -> J -> Response. Xanthine oxidase, dismutation, and the $O_2^-$-driven Fenton reactions generate the reactive oxygen species, i.e. $O_2^-$, $H_2O_2$ and $HO\cdot$. To model the conditions specified by the $O_2^-$ theory, each member of the linear sequence was allowed to interact with $HO\cdot$ while the $O_2^-$ was not indiscriminately reactive, rather it was reacted selectively with only one member of the sequence. The results from this model study clearly show that direct inhibition of one molecule by $O_2^-$ is far more effective in inhibiting the biological process than the more reactive $HO\cdot$ inhibiting all the molecules. Further manipulation of this model clearly show that the key reaction which permits this finding is the Fenton reaction. It appears that the relatively weak production of $HO\cdot$ is "squandered" by ineffective reactions with too many species whereas the higher production of the less reactive $O_2^-$ is "directed" towards the site where it can produce significant inhibition. *Supported by American Heart Association/ Virginia Affiliate.*

**M-Pos461**

EXTRACTION OF AGE RELATED DATA: AN EXAMPLE VIA REGIONAL CEREBRAL BLOOD FLOW AND VASCULAR CO2 REACTIVITY.
Richard P. Spencer, Univ. Connecticut Health Ctr.; Farmington, CT 06032.

Attempts to understand the effects of aging require quantitative data on mechanisms and functional effects. Rather than having to repeat certain studies, or as a guide when further information is needed, it may be feasible to extract age related information from reports already in the literature (studies designed for other purposes, but which contain some age data). As an example, we refer to the study by Tsuda and Hartmann (Stroke 20: 1667, 1989). They used radioxenon (Xe-133) washout to measure blood flow in various regions of the brain, and the effects of administered CO2. Results for their 3 groups were as follows. R = CO2 reactivity, B = blood flow.

R = 0.042 B + 0.329 (mean age 24.3 years)
R = 0.038 B + 0.592 (mean age 33.6 years)
R = 0.035 B + 0.819 (mean age 45.2 years)

The slopes of the lines (S) and the intercepts (I) show age (A) associated progressions, assuming no increasing error with age. For the slope versus age:

S = - 0.332 A + 0.497

That is, the slope falls with age. For the intercept:

I = 0.023 A - 0.220

The intercept goes up with age. Combining formulae, a general expression for CO2 reactivity in terms of blood flow and age can be written.

R = A (0.023 - 0.0332 B) + 0.0497 B - 0.220

As a final step, the equations could be modified, after further data points were available, to include an expression for the percentile. This is because of the probable need to more closely monitor individuals who are beyond certain percentile markers. It may be feasible to extract age related data from multiple literature reports, helping to open "windows" on examining age-related phenomena.

**M-Pos462**

## ON FRACTAL DIMENSIONS OF BRAIN WAVE

Y. Shinagawa, H. Seno, K. Kawano and H. Koito
Dept. Physiol. and Information Processing Center, Nippon Medical School
Tokyo 113, JAPAN

The dimensionality of brain wave has been analized by means of correlation dimension method and another. The correlation dimension shows the dimension of attractor of dynamical system producing the brain wave. Another fractal dimension is obtaind from the graph of brain wave time series.

The dimension of graph, $D$, and that of attractor, $d$, give the number of variables, $N$, in dynamical system producing the brain wave, as follows $N = d - D + 2$.

For the amplitude of brain wave, $x_i$, at time $t_i$, the cumulative path length for a data set can be defined as $\sum_{i=1}^{M-1} |x_{i+1} - x_i|$, where $M$ is the total number of data. If $\log\Delta t$, where $\Delta t$ is the time interval between two nearest data of the amplitude, is plotted against logarithm of the corresponding cumulative path defined above, then the slope gives a fractal dimension of the graph of brain wave: 1·825 ± 0·018 (SD) for frontal α-wave, 1·862 ± 0·03 for occipital. The fractal nature of the graph of brain wave is clear.

The dimension of attractor of occipital α-wave is 3·33 ± 0·14 (SE) and that of frontal α-wave 4·13 ± 0·22; the difference is significant ($p < 0·05$). The number of variables is assumed as 4 for occipital α-wave and 5 for frontal α. These two α-waves must be produced by different dynamical systems.

Those dimensions can be significantly biased due to the condition of subject, for example, who are in Qigong that is a kind of Chinese way of therapy. During Qigong, the dimension of α-wave of subject tends to become larger than in resting: 4·54 ± 0·21 for frontal α-wave, 4·16 ± 0·27 for occipital.

**M-Pos463**

## STATISTICAL NEURODYNAMICS APPROACH TO CENTRAL PATTERN GENERATION

Hong Pan, Jianfeng Feng‡, Minping Qian‡, Aike Guo
(Institute of Biophysics, Academia Sinica, Beijing 100080; ‡ Department of Probability & Statistics, Peking University, Beijing 100871, P.R.China)
(Intro. by L. Stephen Kwok)

Most of the progress in understanding the neural mechanism of animal behavior has come from studying rhythmic behaviors, in which central pattern generator (CPG) have become a key concept, i.e., a specialized assembly of neurons can produce the rhythmic motor output in the absence of both sensory feedback and control by higher neural centers. For a CPG without a pacemaker cell, even knowing the complete neural circuit and all of the cellular and synaptic properties, one does not yet interpret how CPG functions. For this reason, it may be essential to construct the neural network model for descripting the dynamical process in a system of interacting neurons. We have applied the mathematical method of Markov chain with continuous time parameter to the theoritical analysis of CPG. Here we go further into the multiple Markov chain method of the small neural network with multiphasic synaptic connections. This approach is used to analyze and simulate the steady distribution of CPG controlling escape swimming in the marine mollusk Tritonia diomedea. Our results indicate: (1) the steady distribution of this CPG network dynamics mainly concentrates on the cycle, determined by multiphasic synapses which is the major factor of the rhythmic output generated by CPG without pacemaker; (2) the average occupy time at states in this cycle can be estimated by virtue of the cost functionals; (3) even though the delayed excitation from VSI to DSI is not present, Tritonia CPG is still self-sustaining because of the collective property of network dynamics.

**M-Pos464**

## Two-stage Annealing in the Neural Network

Jianfeng Feng Minping Qian
Department of Prob. and Stat., Peking University,
Beijing 100871, P.R.C.

### ABSTRACT

To retrieve memories stored in a neural network, a retrieval procedure called two-stage annealing is proposed. Rigorous theoretical analysis and numerical simulation of the following are given:

1). Trees among the subset of the memories (attractors) can be observed if one applies two-stage annealing in retrieving memories.

2).Suppose that a pattern is a state of a tree. Starting from an information belonging to the attractive basin of any state in the tree, the neural network, undergoing two-stage annealing, will recall the pattern. Result above implies two-stage annealing can dispose of the spurious attractor.

3). 1), 2) hold true for neural network with either asynchoronous dynamic or synchoronous dynamic.

M-Pos465

## DIPOLE ARRAY THEORY PREDICTS NEGATIVE LATERAL STIFFNESS IN MUSCLE

**Tatsuo Iwazumi, Albert Einstein Col. Med., Bronx, NY 10461**

It is well known that the longitudinal stiffness of muscle markedly increases in contraction. This increase has been attributed to increased number of cross-linking between the thick and thin filaments by cross-bridges. However, precipitous reduction of the lateral stiffness in contracting muscle, first observed by Tamura et al (Nature 299, 631-633, 1982) and recently in single sarcomeres by Iwazumi (Biophys. J. 57a, 1990), cannot be explained by the increased number of cross-linking. An electrostatic (dipole array) theory proposed by Iwazumi (1970) predicts that the increase of longitudinal stiffness arises from the gradient of energy density along the thin filament axis while the decrease of lateral stiffness is a result of the dipole array's potential energy which varies with the spacing between thick filaments. A computer simulation of the dipole array indicates that, within the range of physiological spacings, the potential energy has a broad maximum with negative curvatures. The negative curvature, which changes in proportion to dipole energy, results in negative lateral stiffness which varies in proportion to the contractile force. Consequently, the sum of passive and active lateral stiffness diminishes in contraction. The lateral force, which is proportional to the gradient of the potential energy, also changes with the dipole energy but the direction changes with the spacing; inward at short spacings, zero where the potential energy is maximum, and outward at longer spacings. Since the spacing changes with the sarcomere length, the lateral force and stiffness also vary with the sarcomere length. The theory also predicts the effects of troponin on the lateral properties.

M-Pos466

## COOPERATIVE TRANSITIONS AND FEEDBACK INTERACTIONS AS THE BASIS OF A MODEL FOR OSCILLATORY CONTRACTION

**Caroline J. Ritz-Gold and Cliff M. Gold, Biomolecular Sciences, Fremont, California**

**Sustained oscillations have been observed in skeletal muscle as well as in other contractile systems such as insect flight muscle. Although oscillatory contraction in skeletal muscle is thought to be an intrinsic property of the muscle fiber itself, detailed knowledge is still lacking concerning the molecular species and interactions that play a key role in generating these oscillations. In order to gain further insight into this question, we examine models of other oscillatory biological systems. In particular, we focus on certain models of allosteric enzyme systems that are based on cooperative transitions between active and inactive conformational states and on positive feedback interactions such as product activation (e.g., A. Goldbeter et. al., in: "Dynamics of Biochemical Systems," J. Ricard and A. Cornish-Bowden, Eds, 1984).**

**In skeletal muscle, activation and relaxation of contraction is known to be mediated by cooperative transitions of the regulated thin filament. In addition, recent studies have indicated the existence of feedback interactions between cross-bridge attachment to actin and calcium binding to troponin C (A. M. Gordon and E. B. Ridgway, J. Gen. Physiol. 90, 321, 1987). Based on these observations, we develop a kinetic model for oscillatory contraction in which the cooperative properties of the regulated thin filament as well as the feedback interactions between cross-bridge binding and thin filament activation play a key role. We also construct a block diagram representation of this model as a basis for simulating the qualitative features of the observed oscillatory contractile behavior.**

M-Pos467

## CIRCUIT MODELS FOR ELECTRORECEPTION BY FISH*

Leon J. Bruner and James R. Harvey
Department of Physics
University of California
Riverside, CA 92521

Intro. by Jolinda A. Traugh

Certain marine elasmobranch fish are known to be able to detect weak (~5 nV/cm) electric fields in the bandwidth interval, 0.1 - 10 Hz. We have developed a relaxation oscillator model for the electroreceptor organ, the resting frequency of which is modulated to higher or lower values dependent upon the sign and magnitude of applied stimulus. Such behavior closely parallels known electroreceptor response to stimulus. Typical tuning curves obtained from our model circuit are presented and compared with data available from electrophysiological studies[1].

The objectives of our studies are: a) using plausible circuit parameter values, to reproduce physiological values of neural impulse rate in the resting state, b) to duplicate the known bandwidth of response to electric fields, and c) to display a sensitivity to input stimulus comparable to that observed in elasmobranch fish.

1. Murray, R.W., The function of the ampullae of Lorenzini of elasmobranches. In: Lateral Line Detectors. P.H. Cahn, Ed. pp. 277-293. Indiana Univ. Press. 1967

*This work is supported by the Office of Naval Research.

M-Pos468

## STRUCTURE-BASED ANALYSIS OF THE SIEVING BY GELS DURING ELECTROPHORESIS.

Gary A. Griess and Philip Serwer, Department of Biochemistry, The University of Texas Health Science Center, San Antonio, TX 78284-7760.

The sieving during agarose gel electrophoresis of spheres of known radius has been previously used to determine the radius of a gel's effective pore ($P_E$) as a function of the percentage ($A$) of agarose in a gel [Griess et al. (1989) Biopolymers 28, 1475-1484]. For underivatized agarose (Seakem LE, FMC BioProducts) in 0.025 M sodium phosphate, 0.001 M $MgCl_2$: $P_E(A) = P_E(1\%)A^{-0.70}$ when $0.4 \leq A \leq 2.5$. The exponent, -0.7, differs from that expected from a random-fiber gel, -0.5. To determine the relationship of $P_E$ to the structure of agarose gels, the same gels used for measuring $P_E(A)$ were: (a) fixed and stained by use of osmium tetroxide, (b) embedded in epon, (c) thinsectioned, (d) stained with uranyl acetate and then (e) observed by use of electron microscopy. No shrinkage of gels was observed during (a)-(d). Fibers in video images of electron micrographs were skeletonized and one-half the mean distance between contacts with fibers ($P_C$) was determined for random lines passed through the skeleton. In agreement with the observations made for $P_E$, the finding was made that $P_C(A) = P_C(1\%)A^{-0.75}$ when $0.4 \leq A \leq 2.5$; $P_E(1\%)/P_C(1\%)$ was 1.02 for sections with a thickness of 100 nm ± 15%. Deviation from expected random fiber behavior was visible to the eye: regions of comparatively dense fibrous network surrounded comparatively vacant regions. The presence of regions with comparatively small pores explains the previously observed [Griess, G.A. and Serwer, P. (1990) Biopolymers 29, 1863-1866] electrical potential-induced trapping of micron-sized spheres; trapping presumably occurs in the smaller pores.

Supported by NSF (DMB-9003695) and the Robert A. Welch Foundation (AQ-764).

**M-Pos469**

VIDEO MICROSCOPY of SINGLE DNA CHAINS during GEL ELECTROPHORESIS.
Timothy D. Howard and G. Holzwarth. Department of Physics, Wake Forest University, Winston-Salem, NC 27109.

We have digitized sequences of images of individual DNA chains over the first 14 s of agarose gel electrophoresis at 5 V/cm. The intensity-weighted mean position of the center of mass(CM) was computed for each image. From the sequence of images an instantaneous velocity of the CM of individual chains was calculated. This velocity showed large fluctuations in time which correlated with changes in the shape of the chains; molecules in a "U" shape show very low CM velocity. The mean velocity for 10 chains was already 1.5 to 2.0 μm/s after 0.2 s, which reflects a more rapid acceleration than measured previously for a band of T4 DNA in a gel.

To provide a quantitative measure of the changing shape of the chain, the components of the radius of gyration tensor $R_{xx}$, $R_{yy}$, and $R_{xy}$ were also determined from the digitized images, where x is parallel to E. Surprisingly, $R_{xx}$ decreased for the first 1.5 s after E was applied, then increased at longer t.

**M-Pos470**

FURTHER STUDIES OF THE ORIENTATION OF THE AGAROSE GEL MATRIX IN PULSED ELECTRIC FIELDS.
John Stellwagen and Nancy C. Stellwagen, Dept. of Biochemistry, University of Iowa, Iowa City, IA 52242

Transient electric birefringence was used to further characterize the orientation of the agarose gel matrix in pulsed electric fields. Gels ranging in concentration from 0.5% to 1.5% were studied. Pulses varied from 2.5-50 V/cm, with durations ranging up to 50 seconds at the lower voltages. At E = 2.5 V/cm relatively normal positive birefringence signals were observed, characterized by two relaxation times, $\tau_{short}$ ~1-3 s and $\tau_{long}$ ~20 s. These two relaxation times were also observed at higher voltages, but the shape of the birefringence signal changed; the signal was preceded by a long lag period after the pulse was applied and then exhibited a maximum after the pulse was removed before decaying to zero. Steady-state birefringence was not reached if $E \geq 5$ V/cm, even when the pulse duration was increased to 100 s. Reversing the sign of the electric field caused the sign of the birefringence to change from positive to negative, as though orientation of the matrix were occurring in a direction perpendicular to the direction of initial orientation. At $E \geq 25$ V/cm, a negatively birefringent signal with a slower relaxation time was also observed, consistent with the orientation and/or formation of larger aggregates. The repeated use of long orienting pulses frequently caused the whole gel to become optically active and rotate the plane of polarized light by 2-3°. Anisotropic light scattering was also observed under these conditions. These results suggest that large clusters of agarose molecules and/or domains within the matrix can be oriented by pulsed electric fields of the strength and duration commonly used in pulsed electrophoresis experiments. Orientation of the matrix probably contributes substantially to the mechanism of separation of very large DNA molecules in agarose gels by pulsed electric fields. Supported by GM 29690.

**M-Pos471**

ELECTROPORATION BY BIPOLAR ALTERNATING ELECTRIC FIELDS.

Tian Y. Tsong, Piotr Marszalek, Jan Gimsa & T.-D. Xie. Department of Biochemistry, University of Minnesota, St. Paul, MN 55108

Electroporation by alternating electric fields (ac) has been shown to be gentler than direct current (dc) electroporation to the cells. A transfection efficiency of $5.2 \times 10^5$ /$\mu$g DNA was obtained for E. coli (JM105) with plasmid PUC[18] DNA when the cell/DNA mixture was exposed to a 200 V/cm ac field of 30 s duration. This was nearly $10^5$ fold higher than the transfection efficiency of cells which were not exposed to an ac field, although cell survival was identical in both samples. Data also showed that the transfection efficiency was strongly dependent on the frequency of the applied field. The frequency dependence of membrane electroporation was examined by the entry of a fluorescence probe, propidium iodide, into murine myeloma cell line (Tib9). Propidium iodide is weakly fluorescent but becomes strongly fluorescent when bound to DNA. When an ac field reached a critical strength for membrane poration, the dye permeated into the cell. Within a few seconds, two narrow fluorescence bands appeared on the two loci facing the electrodes. The dye diffused into and completely permeated the cells within 2 - 5 min. The critical field strength for membrane poration was found to depend on the ac frequency as described by the Schwan Equation, $\Delta\psi_{crit} = 1.5\, R_{cell}\, E^{\circ}_{crit} / [\,1 + (2\pi f \tau)^{1/2}\,]^2$, in which $\Delta\psi_{crit}$, $R_{cell}$, $E^{\circ}_{crit}$, f, and $\tau$ are the critical membrane breakdown potential, the radius of the cell, the critical amplitude of the applied field, the frequency and the membrane relaxation time, respectively. Electroporation under a rotating ac field was also performed to demonstrate that cell manipulation to produce uniform membrane poration could be achieved under controlled conditions.

[Supported by a grant from Office of Naval Research.]

**M-Pos472**

SURFACE SPECIFIC RECOGNITION OF FLUORESCENT CONJUGATED STREPTAVIDIN-PHYCOERYTHRIN PROTEINS ONTO BIOTIN LIPID LB MONOLAYER FILMS.

L. Samuelson*, P. Miller+, D. Galotti, K.A. Marx, J. Kumar+, S. Tripathy, and D. Kaplan*, *Biotechnology Branch, US Army Natick Labs, Natick, MA 01760; Depts. of Chemistry and +Physics, University of Lowell, Lowell, MA 01854.

The Langmuir-Blodgett technique has been used to simultaneously orient and couple the photodynamic, water soluble protein, phycoerythrin, to a biotin derivatized phospholipid monolayer film. It was found that both avidin and streptavidin phycoerythrin conjugates will preferentially adsorb to the biotinylated lipid monolayer films while at the air-water interface. Pressure-area isotherms indicate that oriented monolayer films are formed with the hydrophilic biotin containing head groups exposed to the four biotin binding sites ($K_a = 10^{15}$) on avidin and streptavidin in the conjugated proteins. The binding of protein to the lipid films was determined by probing the characteristic, intense fluorescence of the phycoerythrin at 576 nm. The measurements were carried out on monolayer films transferred onto solid glass supports, exciting the samples with 496 nm light and scanning the emission from 515 to 670 nm. It was determined that avidin conjugated proteins complex to the biotin lipid monolayer through both specific and non-specific binding mechanisms, while the streptavidin-phycoerythrin binds by what appears to be only a specific (biotin-streptavidin) mechanism. Studies involving the mixture of these biotinylated phospholipids with a conducting polymerized surfactant system have been initiated in an attempt to enhance the stability of the films and elicit novel electronic and optical properties for potential bio-optoelectronic and structural research applications. The results will be presented.

**M-Pos473**

SOLUBILITY OF GASES IN BLOOD PLASMA AT HIGH PRESSURE.

Gary T. Holm, Richard P. Kennan, and Gerald L. Pollack, Department of Physics and Astronomy, Michigan State Univ., East Lansing, MI 48824.

Most of the gas mixture breathed by divers under pressure is inert gas. The solubility and diffusion of inert gases in body fluids are therefore important for understanding decompression sickness. In this paper we discuss measurements of the solubility in blood plasma of three nonreactive breathing gases: helium, nitrogen, and hydrogen. The measurements were carried out in the temperature range 10-37°C at a pressure of about 30 atmospheres, corresponding to a depth of about 300 meters of water. For He, the Ostwald solubility L in blood plasma is about 5-7%, depending on the temperature, smaller than it is in distilled water. The smaller solubility may be a salting-out effect due to the dominant sodium cation in blood plasma. At 25°C we obtained for He the results: L(in plasma)=0.0089 and L(in water)=0.0095. We also report related measurements on the solubility of xenon, in the form of the radioactive isotope Xe-133, at low pressures in blood plasma, blood substitute, and mixtures of blood plasma with blood substitute. The results of the experiments will be analyzed using standard thermodynamic and statistical mechanical methods. Entropies, enthalpies, and Gibbs energies of solubility will be discussed in terms of molecular interactions and compared with other systems.

Supported by ONR-NMRDC Grant No. N00014-88-K-0287.

**M-Pos474**

LIPOSOME-ENCAPSULATED HEMOGLOBIN: USE OF LR16 ANALOGUES IN THE OPTIMIZATION OF ITS OXYGEN BINDING PROPERTIES.

Thomas G. Burke, Yayesh Asmerom+, Alok Singh*, and Sam Rahbar+, Dept. of Medical Oncology and Therapeutics Research, and +Department of Hematology and Bone Marrow Transplantation, City of Hope National Medical Center, Duarte, CA 91010 and *Center for Bio/Molecular Science and Engineering, Naval Research Laboratory, Washington, DC 20375

Reducing the oxygen affinity of liposome-encapsulated hemoglobin (LEH) to a physiologically-optimal range is a key step in the development of an LEH product that may potentially be used as a blood replacement fluid. We have shown that the phenylureido-substituted phenoxyisobutyric acid compound referred to as LR16 [Lalezari et al.(1988) PNAS 85, 617] is effective at modulating the oxygen affinity of purified human hemoglobin microencapsulated in lipid vesicles. In these experiments, hemoglobin was purified from outdated human blood and concentrated to 2.75 mM using pressure ultrafiltration. Hemoglobin solution (1 ml) and LR16 together were encapsulated in synthetic membrane materials (18 mg) consisting of DMPC, DPPC, DSPC, cholesterol and DMPG (ratios of 1:1:1:2.7:0.3, respectively). Liposomes of relatively uniform size (mean diameter between 2-3 um as determined by freeze fracture electron microscopy) were formed by successive extrusions through polycarbonate membrane filters of decreasing pore size. Whereas the $P_{50}$ value for LEH in the absence of drug was 9 mm Hg, the inclusion of LR16 at concentrations of 0.1 mM, 0.2 mM, 0.5 mM, 1 mM, and 1.25 mM resulted in higher $P_{50}$ values of 10 mm Hg, 13 mm Hg, 19 mm Hg, 27 mm Hg and 30 mm Hg, respectively. Thus, the presence of LR16 allows the oxygen dissociation curve of LEH to be right-shifted to a physiologically more relevant $P_{50}$ range. Such a pharmacological approach provides a means of alternating systematically the $P_{50}$ values of LEH formulations. This work was supported by Office of Naval Research Grant No. N00014-90-J-1648 to TGB.

**M-Pos475**

IN-VIVO IMAGING OF $^{99m}$Tc LABELED LIPOSOME ENCAPSULATED HEMOGLOBIN IN AN ANESTHETIZED RABBIT

Alan S. Rudolph[1], William T. Phillips[2], Beth Goins[1], Robert Klipper[2], and Richard O. Cliff[3] [1]Center for Biomolecular Science and Engineering, Naval Research Laboratory, Washington, DC 20375-5000, [2]Department of Nuclear Medicine, University of Texas at San Antonio, San Antonio, TX 78284 [3]GeoCenters Inc. Fort Washington, MD 20744

Liposome encapsulated hemoglobin (LEH) is a hemoglobin-based synthetic red cell substitute which is a potential resuscitative fluid for the in-vivo delivery of oxygen. We have imaged LEH radiolabeled with technetium ($^{99}$mTc) to study the biodistribution in an anesthetized rabbit. Normovolemic rabbits were infused with 30 mls. of a 25mM solution of LEH and imaged under a gamma camera for 2 hours continuously. The rabbits were then allowed to recover from anesthesia and housed until imaged again at 20 hours. The animals were sacrificed and various organs counted to validate the image distribution at 20 hours. The kinetics of LEH biodistribution show rapid uptake by the liver with a slower gradual uptake by the spleen over the course of the experiment. The biodistribution data at 20 hours reveals approximately 50% of the total counts remaining in the blood pool, 17% in the liver, 15% in the spleen, 3% in the bladder and kidney, 2% in the lung, and trace levels in the heart (<1%). We have also examined LEH freeze-dried in the presence of 150 mM trehalose and rehydrated just before labeling and infusion. Similar biodistribution for freeze-dried LEH was observed. These results indicate there is significant circulation persistence of LEH at 20 hours with moderate uptake by the liver and spleen.

**M-Pos476**

BIOPHYSICAL PRINCIPLES USED FOR R AND D OF A NEW PROTEINS SEPARATION METHOD.

Rex Lovrien and Mark Conroy, Biochemistry Dept., Univ. of Minnesota, St. Paul, MN 55108.

Engineers often model proteins as simply particles. Proteins have a 'charge' and a 'size', about all one needs to know for designing any separations method (C and E News, 68, p. 22 (1990)). Belter, Cussler and Hu in Bioseparations (Wiley), 347 (1988) say, quote "bioseparations come from engineering, not science", unquote.(!) Therefore conformational properties and the like can be dismissed in separations design. On the other hand biophysical chemists know about conformational motility, how to measure it in solution. But this information is hardly ever used to design new separations processes or improve old ones.

This poster describes a nearly new method for separations we call Matrix Coprecipitation-Cocrystallization, MCC, or simply Coprecipitation. MCC aims at getting control over conformational motility and solvent penetration of proteins, two factors at the seat of many separations process problems. Three sorts of reactions are key: (i) Properly chosen organic ion ligands in relatively low concentration often tighten protein conformation in solution. (ii) Driven further, organic ligands force precipitation because now one gets inter-ligand attraction, pushing the formation of ligand-protein coprecipitation matrices. (iii) Ligand networks are hosts, proteins are guests. Such coprecipitates, sometimes cocrystals, are relatively dense and low in hydration. This makes MCC products easier to centrifuge, filter, etc. in the engineer's 'unit processes'. MCC was actually invented about 90 years ago (tannic acid precipitation). But the molecular basis for MCC never received much interest nor in most quarters, any comprehension.

The poster also will describe two methods, a 'temperature recycling' method, and a 'distilling method', for driving reactions: Amorphous coprecipitate $\rightarrow$ Crystalline coprecipitate, wherein ligands tighten, order, and protect proteins during the transformation to cocrystals.